

# Mechanisms Underpinning Heterogeneous Deconstruction of Circular Polymers: Insight from Magnetic Resonance Methodologies

Shira Haber,\* Julia Im, Mutian Hua, Alexander R. Epstein, Sophia N. Fricke, Raynald Giovine, Hasan Celik, Kristin A. Persson, Brett A. Helms, and Jeffrey A. Reimer\*



Cite This: <https://doi.org/10.1021/acs.macromol.4c02353>



Read Online

ACCESS |



Metrics & More

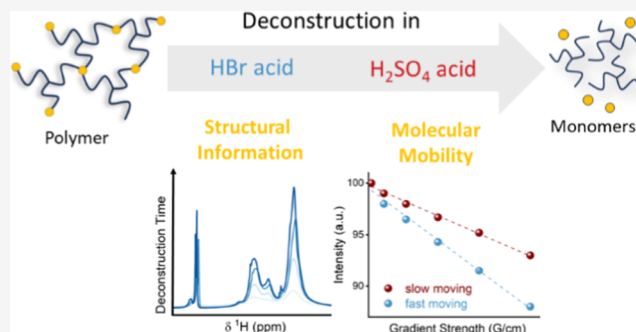


Article Recommendations



Supporting Information

**ABSTRACT:** Circular plastics thrive on the ability to chemically recycle polymers into reusable monomers, ideally closing the loop from manufacturing to the end of life. Mechanisms for polymer deconstruction are complex, involving diffusion and transport of reagents to reactive sites in a material continuously undergoing chemical transformations. A deeper understanding of the deconstruction phenomena would better inform the molecular basis of circularity. Here, we show how nuclear magnetic resonance (NMR) spectroscopy, relaxometry, and diffusometry enable monitoring of the heterogeneous deconstruction of a model elastomer with acid-cleavable diketoenamine bonds. In chaotropic aqueous HBr, polydiketoenamine (PDK) deconstruction is fast, enabled by macro- and microscale swelling, which facilitates acid penetration and protonation of reaction sites deep within the polymer. We observe a previously unrecognized hydrogen-bond-stabilized amine intermediate that is persistent throughout deconstruction. In kosmotropic aqueous H<sub>2</sub>SO<sub>4</sub>, PDK deconstruction is notably slower. Here, swelling occurred at a more gradual pace, characterized by low polymer chain mobility, thereby trapping the acid in matrix pores and modifying the activity of the reaction medium under confinement in the process. We find that polymer swelling, chain mobility, and deconstruction kinetics are strongly linked, requiring a multifaceted NMR characterization tool box for in-depth analysis.



## 1. INTRODUCTION

Circular polymers have emerged as a potential solution to the world's growing disposable plastic waste problem.<sup>1–5</sup> One class of circular polymers is polydiketoenamine (PDK) resins, produced from triketone and amine monomers that condense spontaneously, producing water as the sole byproduct.<sup>6</sup> Deconstruction of these polymers is enabled by a hydrolysis reaction in acid solution, decomposing the material to its initial reusable triketone and amine monomers. The broad palette of triketone and amine monomers available permits the creation of circular thermoplastics, elastomers, and thermosets with unique architectures, as well as useful tunable properties for a range of applications.<sup>1,7</sup> Furthermore, PDK deconstruction is an acid-catalyzed reaction that occurs on spatially and temporally evolving interfaces between two thermodynamic phases and thus poses fundamental questions about nonlinear and nonideal heterogeneous chemical reaction rates. Here, we consider nuclear magnetic resonance (NMR) in its various forms as a noninvasive characterization strategy to study these fundamental phenomena and thus inform circular design of plastics on the basis of both polymers and processes.

PDK (Figure 1a) is an exemplary model system for studying polymer deconstruction. Deconstruction rates are known to be affected by the extent of swelling and ionization of polymer

chains in acidic media, diffusion of reactants and products within the polymer milieu, solvation of ions in complex multicomponent solutions, and the activation of chemically labile bonds.<sup>5,8–12</sup> Heteroatom substitutions<sup>7,13</sup> and spacing along amine and triketone segments<sup>14</sup> also permit tunable fast hydrolysis rates. The initial stage of polymer deconstruction is governed by swelling of polymer chains, while at later stages, the reaction becomes diffusion mediated, enhanced by activation through hydrogen bonds.<sup>15</sup> Strict separation and deconvolution of the various chemical and thermodynamic factors affecting the deconstruction process is challenging, e.g., the nonlinear reaction kinetics being recently described with a fractal-like mathematical model.<sup>16</sup> Nonetheless, a full molecular-level understanding of the deconstruction process is still lacking.

Herein, we monitor molecular transformations of PDK polymers during acid deconstruction by NMR techniques.

**Received:** September 26, 2024

**Revised:** December 15, 2024

**Accepted:** January 3, 2025

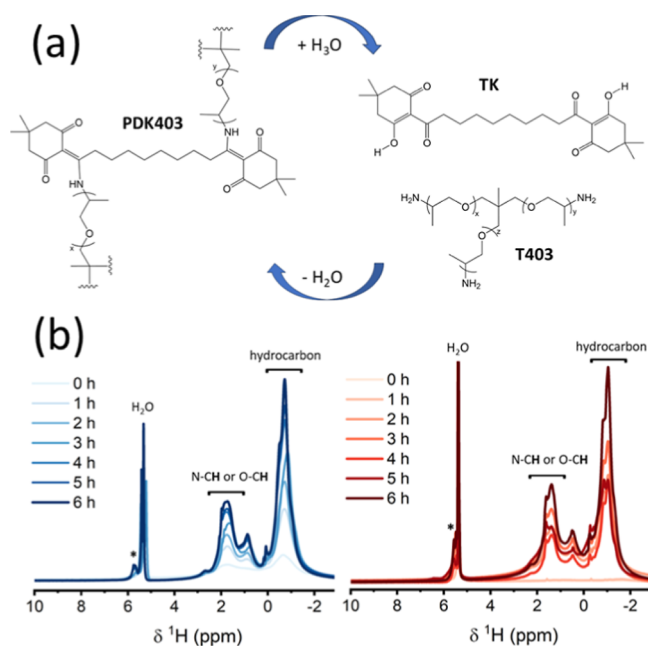


**Figure 1.** (a) Chemical structure of the deconstruction of PDK403 to its monomers, triamine polypropylene glycol cross-linker (T403), and triketone (TK) and the circular process to create PDK403. (b) In situ solution-state  $^1\text{H}$  NMR measurements of PDK403 in 5 M DBr/ $\text{D}_2\text{O}$  (blue) and  $\text{D}_2\text{SO}_4/\text{D}_2\text{O}$  acid (red) solutions performed at 11.7 T. Chemical environment regions and water peaks are labeled. An asterisk marks the presence of a new environment.

Two acidic solutions were selected: HBr, a chaotropic agent enhancing polymer–water interactions, and  $\text{H}_2\text{SO}_4$ , a kosmotropic agent, increasing surface tension due to low polymer–water interactions.<sup>12,17,18</sup> Consistent with previous bulk studies,<sup>15,16</sup> we find deconstruction rate constants for PDK to follow  $k_{\text{HBr}} > k_{\text{H}_2\text{SO}_4}$ . At episodic intervals, we quenched the HBr deconstruction of PDK polymers to employ  $^1\text{H}$  and  $^{13}\text{C}$  solid-state NMR (ssNMR) spectroscopy to probe the chemical structure of the recovered deconstructed polymer. A combination of solution- and solid-state multinuclear NMR, together with DFT calculations, reveals in the KBr reaction an intermediate that inhibits further monomer formation and thereby slows the deconstruction reaction. Ameliorating this intermediate provides a key insight into design of more rapidly degrading PDK constructs. We further use relaxometry and diffusometry NMR methods to assess the molecular mobility of PDK and its fragments as a function of deconstruction time, thereby revealing the mobility of specific chemical environments throughout the activation of the diketoenamine (DKE) bond. Our results point to a previously unrecognized mechanism for ensuring circularity in plastics undergoing heterogeneous deconstruction: control over local chain mobility is critical in overcoming barriers in accessing reactive conformations. Our results also suggest that there are molecular-informed strategies for codesigning polymers and processes to deliver reusable monomers in high yield and purity at fast overall rates by considering macromolecular dynamics and conformation.

## 2. MATERIALS AND METHODS

**2.1. Materials.** PDK elastomers were synthesized by vortex mixing a triketone monomer (1,10-bis(2-hydroxy-4,4-dimethyl-6-oxocyclohex-1-en-1-yl) decane-1,10-dione)<sup>6</sup> with tribranched amine-termi-

nated polypropylene glycol cross-linkers T403, T3000, and T5000 (Huntsman), whose molar masses are nominally 440, 3000, and 5000  $\text{g mol}^{-1}$ , respectively. A detailed description has been previously reported.<sup>15</sup> It should be noted that PDK403 is a model system polymer. Due to the moderate molecular weight of the polymer under investigation, realistic systems may show different results and need to be investigated.

Acids were prepared in 5 M concentration of HBr, HCl, and  $\text{H}_2\text{SO}_4$  (Sigma-Aldrich) and DBr/ $\text{D}_2\text{O}$ ,  $\text{D}_2\text{SO}_4/\text{D}_2\text{O}$ , and DCl/ $\text{D}_2\text{O}$  (Thermo Scientific).

DKE was synthesized as previously described.<sup>15</sup> Briefly, the monotopic triketone monomer<sup>6</sup> was mixed with 1-methoxy-2-propylamine at 60 °C for 2 h to yield an off-white solid.  $\text{CDCl}_3$ ,  $\text{DMSO-}d_6$ , and  $\text{D}_2\text{O}$  were purchased from Cambridge Isotope Laboratories, Inc. Sodium hydroxide (Sigma-Aldrich) solution was prepared at a 5 M concentration.

**2.2. Sample Preparation.** For in situ NMR experiments: a cylindrical punch of PDK403, with a diameter of 4 mm and height of 1 mm, was placed in a 5 mm NMR tube with 400  $\mu\text{L}$  of deuterated acid.

For ex-situ ssNMR experiments: a cylindrical punch of the polymer, with a diameter of 8 mm and height of 1 mm, was placed in a 25 mL scintillation vial equipped with a stir bar and 4 mL of 5 M acid. After desired amount of time, the solid polymer was filtered, washed with excess amount of acid, then with excess amount of water, and placed in a vacuum oven at 60 °C for overnight drying. The outermost layers of the recovered polymer were chopped up and ground and packed into rotors. Pristine PDK403 was sliced into very small pieces and placed in a rotor.

For solution NMR measurements: samples were prepared for *ex-situ* ssNMR, then the outermost layers of the recovered polymer were chopped up, placed in an NMR tube, and dissolved in  $\text{DMSO-}d_6$  or  $\text{CDCl}_3$ . For  $^1\text{H}$ – $^{15}\text{N}$  heteronuclear single quantum coherence (HSQC) measurement, a 3 mm NMR tube was used to maximize the sample concentration with minimal solvent.

Small molecule deconstruction study of DKE was performed by placing 10 mg of DKE in a vial with 500  $\mu\text{L}$  of 5 M DCl/ $\text{D}_2\text{O}$ . After the desired amount of time, an aliquot of 200  $\mu\text{L}$  was extracted and thoroughly mixed with 400  $\mu\text{L}$  of  $\text{DMSO-}d_6$ . The  $\text{DMSO-}d_6$  phase was separated and placed in a 5 mm NMR tube for testing.

For acidity testing: an 8 mm cylinder with a height of 1 mm of PDK403 was placed in 4 mL of 5 M HBr or 5 M  $\text{H}_2\text{SO}_4$  with a stir bar. After desired amount of time, the recovered polymer was filtered and placed in 5 M NaOH for 30 min, then filtered, washed with base and water, and dried overnight under vacuum at 60 °C.

Preparation for diffusion measurements: a long slice (~20 mm) of PDK403, weighing 19–22 mg, was placed in a 4 mm PTFE liner with 200  $\mu\text{L}$  of 5 M DBr/ $\text{D}_2\text{O}$  or 5 M  $\text{D}_2\text{SO}_4/\text{D}_2\text{O}$ . The liner was placed in a 5 mm NMR tube. After the temperature was stable (298 K),  $^1\text{H}$  PFG-NMR measurements were performed.

**2.3. Solution NMR Measurements.**  $^1\text{H}$  and  $^{13}\text{C}$  chemical shifts were referenced with respect to tetramethylsilane, with  $\text{CDCl}_3$  ( $^1\text{H}$  at 7.26 ppm and  $^{13}\text{C}$  at 77.16 ppm) or  $\text{DMSO-}d_6$  ( $^1\text{H}$  at 2.50 ppm and  $^{13}\text{C}$  at 39.52 ppm).

In situ experiments were performed on an 11.7 T AVANCE I NMR spectrometer (500.23 MHz for  $^1\text{H}$  and 125.78 MHz for  $^{13}\text{C}$ ) at room temperature. For  $^1\text{H}$  measurements, the zg30 Bruker pulse program was used with relaxation delay of 5 s and 16 scans. For  $^{13}\text{C}$  measurements, the zgpg30 Bruker pulse program was used with a relaxation delay of 1 s with 512 scans. RF fields were 27.78 and 29 kHz for  $^1\text{H}$  and  $^{13}\text{C}$ , respectively.

An 11.7 T Bruker AVANCE IV NEO Console equipped with a 5 mm BBO Prodigy CryoProbe (500.17 MHz for  $^1\text{H}$ ) was used for  $^1\text{H}$ – $^1\text{H}$  Correlation Spectroscopy (COSY) measurement for recovered PDK403 (Bruker program cosygpppqf) with a relaxation delay of 2 s and 4 scans. 2048 data points were acquired for the direct dimension with 256 increments.  $^1\text{H}$ – $^{15}\text{N}$  HSQC measurement for recovered PDK403 was performed on the same instrument (Bruker program hsqcetspsi2) with Echo-Antiecho TPPI acquisition mode, a relaxation delay of 2 s, 96 scans, and 2048 data points in the direct

dimension with 192 increments. RF fields of 20.8 and 16.67 kHz were used for  $^1\text{H}$  and  $^{15}\text{N}$  nuclei, respectively.

$^1\text{H}$ – $^1\text{H}$  COSY for small-molecule DKE and  $^1\text{H}$ – $^1\text{H}$  Nuclear Overhauser Effect Spectroscopy (NOESY) for DKE and recovered PDK403 were acquired on an 11.7 T Bruker AVANCE IV NEO Console equipped with a 5 mm iProbe (499.997 MHz for  $^1\text{H}$  and 125.72 MHz for  $^{13}\text{C}$ ). Relaxation delay of 2 s, 8 scans, and mixing time of 0.6 s were used with Bruker pulse programs cosyppppqf and noesygpph, respectively, and with TPPI acquisition mode for the latter. 2048 data points were acquired for the direct dimension with 256 increments.  $^1\text{H}$ – $^{13}\text{C}$  HSQC was measured using a relaxation delay of 2 s with 16 scans using the Bruker pulse program hsqcetgpsisp2.2 and Echo-Antiecho TPPI acquisition mode. 2048 data points were acquired for the direct dimension with 256 increments. An RF field of 32.26 and 23.8 kHz was used for  $^1\text{H}$  and  $^{13}\text{C}$ , respectively.

$^{15}\text{N}$  measurements were acquired on a 14.1 T Bruker spectrometer, equipped with a Bruker AVANCE III console and a 5 mm BBO Prodigy CryoProbe (600.13 MHz for  $^1\text{H}$  and 60.81 MHz for  $^{15}\text{N}$ ). Data was acquired using the Bruker pulse program zgig with a relaxation delay of 5 s and 192 scans.  $^{15}\text{N}$  chemical shift was referenced to a solution of 90% nitromethane,  $\text{NO}_2\text{CH}_3$  (TCI): 10%  $\text{CDCl}_3$  (Cambridge Isotope Laboratories, Inc.) at 380 ppm. In addition, selective NOESY measurements were performed on this magnet, with a Bruker pulse program selnogps2, relaxation delay of 5 s, mixing time of 0.6 and 2 s, with 608 and 128 scans, respectively.

Variable-temperature (288 K–318 K)  $^1\text{H}$  measurements for recovered PDK403 were acquired on a 9.4 T Bruker AVANCE IV NEO console (400.23 MHz for  $^1\text{H}$ ) that is equipped with a double-resonance broad band diffusion (diffBB) probe and a cooler unit (BCU-II). After the temperature was stable, the zg30 Bruker pulse program was used with relaxation delay of 5 s and 16 scans.

Pulsed-Field Gradient (PFG) diffusion NMR measurements: Self-diffusion coefficients were measured using PFG-NMR at a field strength of 9.4 T on a Bruker AVANCE IV NEO (400.23 MHz for  $^1\text{H}$ ) spectrometer fitted with a 5 mm water-cooled double-resonance diffBB probe equipped with z-axis gradient and a cooler unit (BCU-II). Sample temperatures and gradient strengths were calibrated using an ethylene glycol sample (80%) in  $\text{DMSO}-d_6$  (20%) and maintained at 298 K throughout measurements. A standard stimulated echo sequence (diffSTE) using sine-bell magnetic field gradient pulses was employed with application of 8 dummy gradient pulses at the beginning of each program prior to spectral acquisition and 16 dummy scans. Gradient strengths of up to 1000 G/cm in 16 equally spaced increments to achieve optimal signal attenuation were employed. All gradient pulse pairs had a duration ( $\delta$ ) of 1 ms and a diffusion time ( $\Delta$ ) of 20 ms. A relaxation delay of 5 s was used for all experiments.

The attenuation curve was fit to the Stejskal–Tanner equation

$$S(g) = S(0) \exp \left[ -D \times \gamma^2 g^2 \delta^2 \left( \Delta - \frac{\delta}{3} \right) \right] \quad (1)$$

where  $S(g)$  is the integrated signal at gradient strength  $g$ ,  $D$  is the self-diffusion coefficient,  $\gamma$  is the gyromagnetic ratio,  $\delta$  is the gradient encoding duration, and  $\Delta$  is the diffusion delay.<sup>19</sup> Data was processed with Bruker TopSpin 4.1.4 and 4.3.0 and Bruker Dynamics Center 2.8.0.1 and 2.8.4.

Inverse Laplace transform (ILT) was performed in MATLAB (MathWorks, Natick, MA), with NNLS algorithm and optimal regularization using the L-curve method.<sup>20</sup> The smoothing parameter,  $\mu$ , was chosen after optimization for each individual experiment by manually finding the corner value generated from the L-curve. MATLAB code files have been deposited on the Reimer group Web site (<https://reimergroup.org/data.html>).

**2.4. ssNMR Experiments.**  $^1\text{H}$  and  $^{13}\text{C}$  ssNMR spectra were recorded at 9.4 T using a Bruker BioSpin spectrometer equipped with an AVANCE IV Neo console and 3.2 or 1.3 mm double-resonance HX magic angle spinning (MAS) probes that tune to both  $^1\text{H}$  (400.1 MHz) and  $^{13}\text{C}$  (100.6 MHz).

Samples were loaded in 3.2 or 1.3 mm zirconia rotors, closed using Vespel caps, and spun at the magic angle at spinning speeds of 11 or 50 kHz using dry nitrogen. Sample weight varied between 14 and 28 mg for 3.2 mm and between 2.1 and 3.6 mg for 1.3 mm.

$^1\text{H}$  ssNMR spectra were obtained by using a rotor-synchronized Hahn echo sequence ( $90^\circ - \tau_R - 180^\circ - \tau_R - \text{AQ}$ ) with an RF field of 119 kHz.  $T_1$  relaxation measurements were acquired using a saturation recovery pulse sequence followed by echo detection. The initial saturation of  $^1\text{H}$  magnetization was achieved by using a train of 100 short  $90^\circ$  pulses (119 kHz) spaced by 3 ms. For quantitative  $^1\text{H}$  Hahn echo spectra, relaxation delay of 12 s was used which was long enough to reach full relaxation of all  $^1\text{H}$  signals in all samples with 16 scans. Transverse relaxation,  $T_2$ , was measured with a spin echo pulse sequence using an echo delay of 20–40  $\mu\text{s}$ . Relaxation time  $T_{1\rho}$  was measured at room temperature with a standard spin-lock experiment ( $90^\circ$  pulse immediately followed by a phase-shifted variable-length spin-locking pulse) with an RF spin-lock field of 80 kHz.  $^{13}\text{C}$  cross-polarization (CP) experiments under the Hartmann–Hahn matching condition were performed with a relaxation delay of 2 s and varying contact periods between 0.5 and 4 ms. During  $^{13}\text{C}$  acquisition, high-power  $^1\text{H}$  decoupling was applied using the 83 kHz SPINAL-64<sup>21</sup> (Small-Phase Incremental Alternation with 64 steps) decoupling scheme. Quantitative  $^{13}\text{C}$  multi cross-polarization (multiCP) experiments were obtained using the multiCP sequence developed by Schmidt-Rohr and co-workers.<sup>18,22,23</sup> Recovery delay was optimized for each sample,  $5 \times T_1$ , varying from 2.3 to 5 s, as was the intercontact delay,  $2 \times T_1$ , varying from 1 to 2 ms. The same CP conditions for  $^{13}\text{C}$  CP measurements were used with multiCP. Contact time (1–2 ms) was divided into 11 contact periods of 90 or 180  $\mu\text{s}$  each, respectively. During  $^{13}\text{C}$  acquisition, high-power  $^1\text{H}$  decoupling was applied using the 83 kHz SPINAL-64 decoupling scheme. RF fields of 95 and 74 kHz were used for  $^1\text{H}$  and  $^{13}\text{C}$ , respectively.

$^1\text{H}$  and  $^{15}\text{N}$  ssNMR spectra were recorded at 11.75 T (500.1 MHz for  $^1\text{H}$ ) using a Bruker BioSpin spectrometer equipped with an AVANCE-I console and 4.0 mm double-resonance HX MAS probes that tune to both  $^1\text{H}$  (500.1 MHz) and  $^{15}\text{N}$  (50.69 MHz). Samples were loaded in 4.0 mm zirconia rotors, closed using Kel-F caps, and spun at the magic angle with a spinning speed of 5 kHz using dry nitrogen.

$^1\text{H}$ – $^{15}\text{N}$  CP experiments under the Hartmann–Hahn matching condition were performed with a recovery delay of 2 s, contact time of 2 ms, and 50 kHz TPPM  $^1\text{H}$  decoupling during signal acquisition. RF fields were 61 and 50 kHz for  $^1\text{H}$  and  $^{15}\text{N}$ , respectively.

$^1\text{H}$  and  $^{13}\text{C}$  chemical shifts were referenced with respect to tetramethylsilane using the  $\text{CH}_2$  resonance of adamantane as a secondary external reference at  $^{13}\text{C} = 38.48$  ppm and  $^1\text{H} = 1.8$  ppm.  $^{15}\text{N}$  was referenced to glycine at 33.4 ppm.<sup>24</sup>

All solution and ssNMR data were processed using Bruker TopSpin 4.1.4 and 4.3.0 and DMfit software.<sup>25</sup>

**2.5. DFT Calculations.** All hybrid-DFT calculations were performed using Gaussian16 and GaussView.<sup>26</sup> The geometry of each molecule was optimized at the B3LYP/6-311+G(d,p) level of theory with the D3 dispersion correction added.<sup>27,28</sup> NMR tensors were calculated at the B3LYP/6-311+G(2d,p) level of theory using the Gauge-Independent Atomic Orbital method, as implemented in Gaussian16.  $^1\text{H}$  and  $^{13}\text{C}$  NMR shifts were calculated using a TMS B3LYP/6-311+G(2d,p) reference, and  $^{15}\text{N}$  NMR shifts were calculated using a  $\text{NH}_3$  B3LYP/6-311+G(2d,p) reference. For thermodynamic values, the molecule optimization and vibrational frequencies were calculated at the wB97XD/6-311+G(d,p) level of theory.<sup>29</sup> Free energies were calculated using standard thermochemistry as implemented in Gaussian16, with the exception of the vibrational entropy, which was calculated using the Quasi-Rigid Rotor Harmonic Oscillator approximation.<sup>30</sup>

### 3. RESULTS AND DISCUSSION

We monitored acid deconstruction of a PDK elastomer (PDK403) prepared from a simple ditopic TK monomer and a triamine

polypropylene glycol cross-linker with an average molar mass of  $440 \text{ g mol}^{-1}$  (T403) in an acidic medium via NMR three methods, each chosen to highlight the structure and dynamics of reactants, products, and intermediates. First, we carried out in situ solution-state NMR, probing the small molecules being released in solution during the course of the reaction. Solution-state NMR spectroscopically discriminated against unreacted polymer because the early stages of PDK403 deconstruction in acid exhibit a hydrophobic polymer with a minimal  $^1\text{H}$  solution-state NMR signal. As deconstruction progresses, the soluble intermediates show an increase in NMR signal intensity, governed by their acid solubility, until the TK final monomer, an insoluble solid, precipitates and the solution-state NMR signal is lost. The rise and fall of these solution-state NMR signals thus follows soluble reaction intermediates. Second, we carried out multinuclear ssNMR measurements on selected solid polymer samples deconstructed for specific reaction times. Here, the deconstructed polymer, consisting of only the distended outer layer of material that reacted with the acid, was subject to the ssNMR experiments. Third, we turned to relaxometry and diffusometry methods to probe polymer and solvent mobility, including spin–lattice relaxation measurements in the rotating frame ( $^1\text{H}$   $T_{1\rho}$  relaxation) and in situ PFG NMR. The purpose here is to diagnose the relationship between dynamics and morphological heterogeneity of the polymer during the deconstruction process.

**3.1. In Situ Solution-State Characterization.** A circular punch (8 mm diameter and 1 mm height) of the PDK403 elastomer (Figure 1a) was placed in 5 M deuterated acid solution in an NMR tube and monitored hourly with solution-state  $^1\text{H}$  NMR (Figure 1b). Note that a shift of  $\sim 2$  ppm upfield of the proton resonances occurs as a result of the presence of the highly concentrated acids (Figure S1).

At  $t = 0$  h (the time of acid addition), a very small solution-state  $^1\text{H}$  signal is detected for the polymer in both acid solutions, as expected for the insoluble hydrophobic PDK403 polymer ( $^1\text{H}$  NMR spectrum of PDK403 in  $\text{D}_2\text{O}$  can be found in Figure S2). Organic solvents lead to swelling of the polymer chains and do not further dissolve the polymer (Figure S3). As deconstruction progresses, growth in proton signals emanating from the hydrocarbon region,  $-2$  to  $0.5$  ppm ( $0$ – $2.5$  ppm in  $\text{CDCl}_3$ , Figure S1), and the heteroatom region ( $\text{N}-\text{CH}$  and  $\text{O}-\text{CH}$ ),  $1$  to  $3$  ppm ( $3$ – $5$  ppm in  $\text{CDCl}_3$ , Figure S1), is evident. These increases are the result of polymer protonation, further solvation, and a decrease in hydrophobicity. Spectral differences between the two acids are not seen with these liquid-state NMR measurements.

Interestingly, a peak resonating at  $5.5$  ppm in  $\text{D}_2\text{SO}_4$  and  $5.8$  ppm in  $\text{DBr}$  (Figure 1b, asterisk) emerges and grows with the reaction time. The chemical shift suggests that this peak emanates from the protonated amine that detaches from the polymer. Indeed, the protonated state of the cross-linker monomer T403 ( $-\text{NH}_3^+$ ) is soluble in both acids (Figure S4). TK monomers, however, are not soluble in acid solutions and precipitate or float to the acid surface. Figure S5 shows the lack of the  $^1\text{H}$  signal from the measurement of TK in deuterated acid/ $\text{D}_2\text{O}$  as compared to the  $^1\text{H}$  spectrum of TK in  $\text{CDCl}_3$ . We conclude that the molecular origin of the new peak is unclear from these solution NMR data alone, and the differing solubilities of the various species (polymers, monomers, and deconstructed intermediates) during the deconstruction process obfuscate simple analysis.

**3.2. Polymer Deconstruction Pathways from Ex-Situ ssNMR.** In-depth investigation of polymer deconstruction, with high resolution and high sensitivity, was enabled with multinuclear ssNMR measurements performed on deconstructed polymer samples that consist of only the distended outer layer of material that reacted with acid (detailed sample preparation can be found in the Materials and Methods Section and Figure S6). Figure S7 shows the comparison of in situ and *ex-situ* NMR spectra for  $^1\text{H}$  and  $^{13}\text{C}$  measurements, demonstrating that the integrity of the sample remains with both measurement setup conditions. Figure 2a,b shows the quantitative  $^1\text{H}$ – $^{13}\text{C}$  multiCP<sup>18,22,23</sup> measurements of the recovered deconstructed polymer in 5 M HBr and 5 M  $\text{H}_2\text{SO}_4$ , respectively. Four regions of interest have been labeled as follows: methylene  $\text{CH}_x$

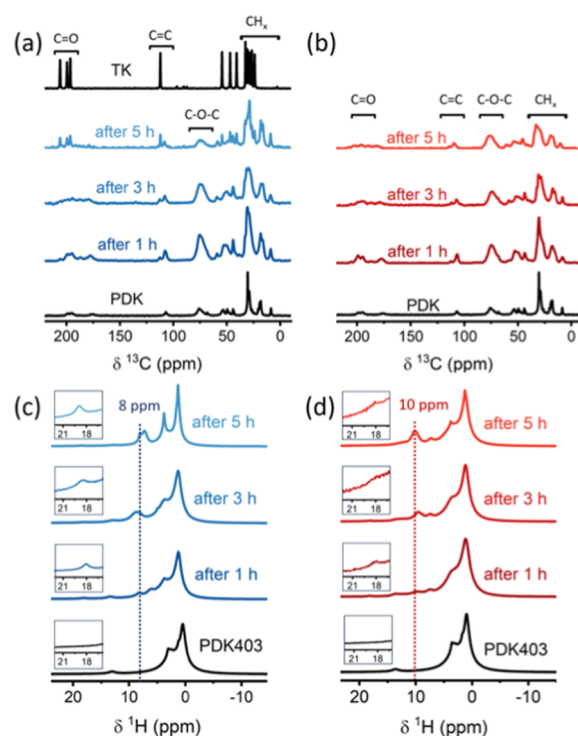


**Figure 2.**  $^1\text{H}$ – $^{13}\text{C}$  multiCP spectra of recovered PDK403 after different deconstruction times in (a) 5 M HBr solution (blue) and (b) 5 M  $\text{H}_2\text{SO}_4$  solution (red) acquired at 9.4 T. Various chemical environments are labeled. Normalization according to the number of scans and sample weight was performed.  $^1\text{H}$  Hahn echo spectra of recovered PDK403 after different deconstruction times in (c) 5 M HBr solution (blue) and (d) 5 M  $\text{H}_2\text{SO}_4$  solution (red) acquired at 9.4 T. Insets magnify the 18 ppm peak assigned to the monomer enol proton environment. Normalization was performed according to the number of scans and sample weight.

moieties resonating at  $0$ – $40$  ppm that correspond to carbons of the polymer chains;  $\text{C}-\text{O}-\text{C}$ , ether carbons resonating at  $65$ – $75$  ppm;  $\text{C}=\text{C}$  double bonds resonating at  $105$ – $115$  ppm; and  $\text{C}=\text{O}$ , carbonyls resonating at  $170$ – $210$  ppm. Clear changes in carbon environments are evident as a function of polymer deconstruction time in HBr.

Peaks associated with methylene  $\text{CH}_x$  groups become broader with reaction time, yet after 5 h, they sharpen and narrow (vide infra). The ether region's signal intensity decreases with time, likely a result of elimination of the protonated amine cross-linker. After one h in acid, new peaks emerge that originate from TK monomer formation (shown in the first stacked row), growing in intensity as deconstruction advances. As the reaction proceeds past five h, polymer chain line widths decrease, particularly for the HBr-reacted system. This is presumed to be associated with increased mobility of the monomer-like  $\text{CH}_x$  bonds, further supporting the enhanced deconstruction rate of PDK in the HBr acid medium, and will be discussed further. In comparison, the  $^{13}\text{C}$  spectra of the deconstructed polymer in  $\text{H}_2\text{SO}_4$  acid show very subtle changes. A small peak at  $112$  ppm ( $\text{C}=\text{C}$  bond) emerges after 1 h, but does not grow with deconstruction time, indicating that hydrolysis is taking place but at a much slower rate.

Enhanced deconstruction kinetics in HBr vis-à-vis  $\text{H}_2\text{SO}_4$  can also be seen from fast MAS quantitative  $^1\text{H}$  Hahn echo measurements plotted in Figure 2c,d. We chose to obtain these spectra with a Hahn echo sequence due to the recovery time of the MAS probe; the echo time was found, however, to be short relative to the measured  $T_2$  values (see Table S5), thus enabling acquisition of quantitative data. PDK403 shows two broad overlapping peaks in the  $0$ – $4$  ppm region, corresponding to  $\text{CH}_3$ ,  $\text{CH}_2$ , and  $\text{CH}_2-\text{O}$  bonds, and an amine

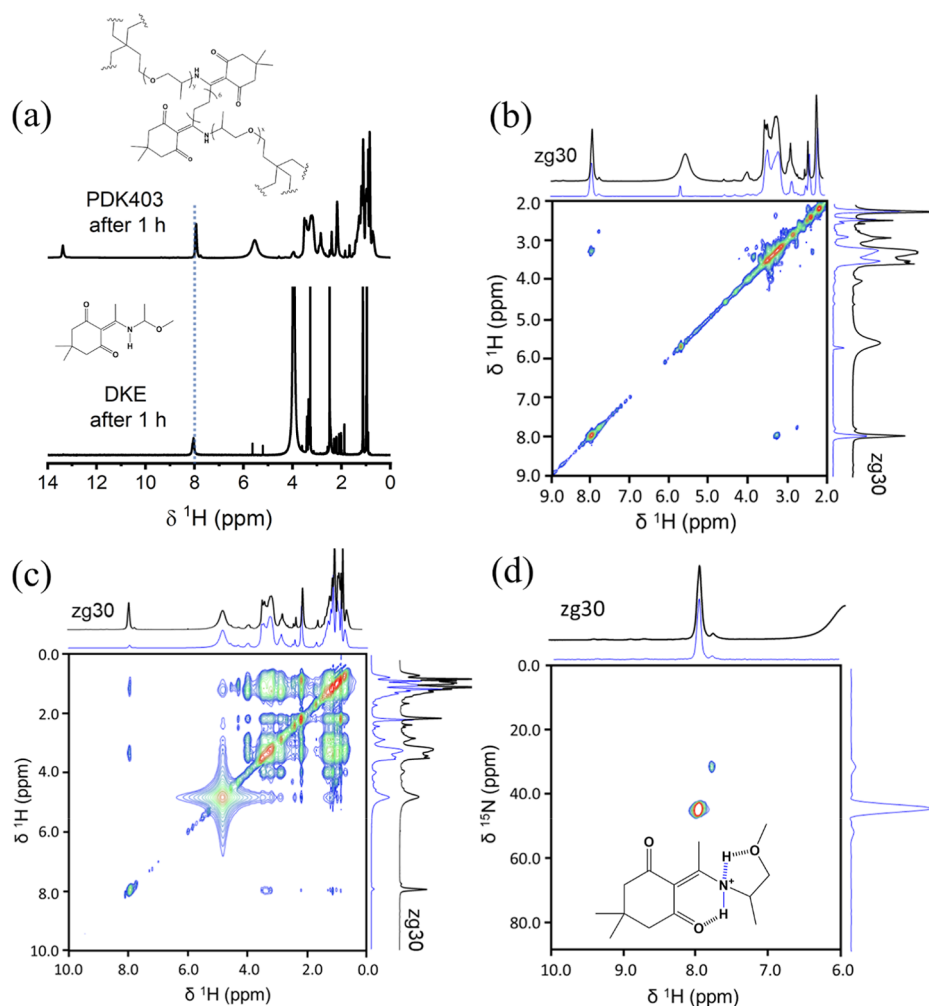


**Figure 3.** (a)  $^1\text{H}$  spectra of recovered DKF after 1 h in 5 M HCl, extracted with  $\text{DMSO-}d_6$  (bottom spectrum) and the solid sample of recovered PDK403 after 1 h in 5 M HBr dissolved in  $\text{DMSO-}d_6$ . (b)  $^1\text{H}$ – $^1\text{H}$  COSY measurement of the recovered polymer after 1 h in 5 M HBr dissolved in  $\text{DMSO-}d_6$ . A cross peak can be seen between  $^1\text{H}$  at 8 ppm and  $^1\text{H}$  at 3.4 ppm, the latter assigned to a  $\text{CH}_2\text{--O}$  site. (c)  $^1\text{H}$ – $^1\text{H}$  NOESY measurement of the recovered polymer after 1 h in 5 M HBr dissolved in  $\text{DMSO-}d_6$ . Two cross peaks with 8 ppm are evidenced: the first correlates with 3.4 ppm, assigned to a  $\text{CH}_2\text{--O}$  site, and the second cross peak correlates to  $^1\text{H}$  at 8 ppm with 1.2 ppm, assigned to the hydrocarbon group of the methylene chain. (d)  $^1\text{H}$ – $^{15}\text{N}$  HSQC correlation of the recovered polymer after 1 h in 5 M HBr dissolved in  $\text{DMSO-}d_6$ . Inset shows the proposed structure of the intermediate material formed during deconstruction. A central cross peak is attributed to the  $^{15}\text{N}$ – $\text{H}$ – $\text{O}$  site at 45 ppm correlating with  $^1\text{H}$  at 8 ppm as discussed in the main text and [Supporting Information](#). Spectra were acquired at 11.7 T.

proton peak that resonates at 13.6 ppm. After 1 h of deconstruction in both acids, a new peak emerges at 18 ppm, which is assigned to the enol proton of the TK monomer (Figures 1a and S8). Two small new proton peaks are observed in the  $\text{H}_2\text{SO}_4$  deconstruction (red). The first peak, resonating at 7.4 ppm, is assigned to the protonated amine,  $-\text{NH}_3^+$  (Figure S4). This peak is also seen with in situ monitoring of the reaction in deuterated sulfuric acid in Figure 1b (note that the peak is shifted upfield due to a high concentration of acid). In addition, a second new peak appears at 9.85–10.1 ppm, shifting downfield and increasing in intensity as deconstruction progresses. This peak is assigned to residual  $\text{HSO}_4^-$  that is trapped in the newly formed pores of the deconstructed polymer<sup>31</sup> (refer to Figures S9 and S10 for additional confirmation). As deconstruction advances, the polymer matrix swells slowly, enabling larger volumes of acid to penetrate through the polymer chains; this acid is then captured during the reaction quenching process. The increase in residual acid intensity is supplementary evidence that the system undergoes molecular swelling and expansion with increased porosity. This swelling is further discussed in the context of NMR relaxation and diffusion. This analysis leaves one  $^1\text{H}$  NMR peak unassigned.

Polymer deconstruction in HBr acid (Figure 2c) leads to the evolution of a distinct proton environment at 8–9 ppm. Given the

efficient protonation abilities of the amine reaction site, we suggest that the 8–9 ppm peak is associated with the formation of a rather stable intermediate that remains in the reaction medium even after 5 h of deconstruction time. This intermediate is also formed in the deconstruction of additional PDK formulations with structurally similar cross-linkers yet varying in molar mass (Figure S11) and does not change with varying temperature or after a base treatment (Figures S12 and S13), demonstrating its relative stability. The question remains as to the identity of an intermediate that presents itself as an  $\sim 8$  ppm proton NMR peak in HBr depolymerization.

Assignment of this intermediate peak prompted a comparative study of the deconstruction of PDK403 and the equivalent small molecule DKF in acid. Figure 3a presents  $^1\text{H}$  solution-state NMR spectra (materials dissolved in  $\text{DMSO-}d_6$ ) of recovered small molecules and polymer after 1 h in acid solution, showing a clear presence of the 8 ppm proton environment.  $^1\text{H}$ – $^1\text{H}$  2D COSY and NOESY measurements were performed for both samples, with comparable cross peaks (Figure 3b,c, S15, and S16). The proton environment is coupled through bonds to the proton adjacent to the ether group,  $\text{CH}_2\text{--O--CH}_2$ , and through space to the protons in the methylene chain (see the Supporting Information for detailed cross

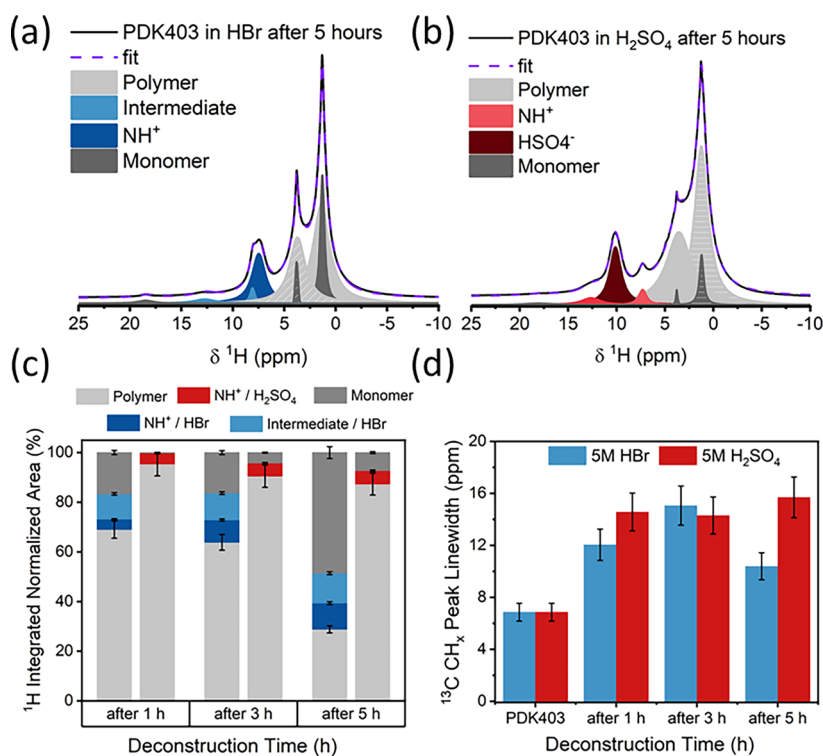


**Figure 4.** Deconvolution of the  $^1\text{H}$  Hahn echo spectrum of PDK403 after 5 h in (a) 5 M HBr acid and (b) 5 M  $\text{H}_2\text{SO}_4$  acid acquired at 9.4 T. Environments were separated into three groups according to the chemical shift and peak line width (colors). (c) Integration of deconvoluted normalized  $^1\text{H}$  Hahn echo spectra (Figure 2c,d) of recovered PDK403 in 5 M HBr (blue) and 5 M  $\text{H}_2\text{SO}_4$  (red) acid solutions as a function of deconstruction time. (d) Peak line width of the  $^{13}\text{C}$  chemical shift region of 0–30 ppm, corresponding to carbon resonance from polymer chains, was fit and plotted vs deconstruction time in 5 M HBr acid (blue) and  $\text{H}_2\text{SO}_4$  acid (red).

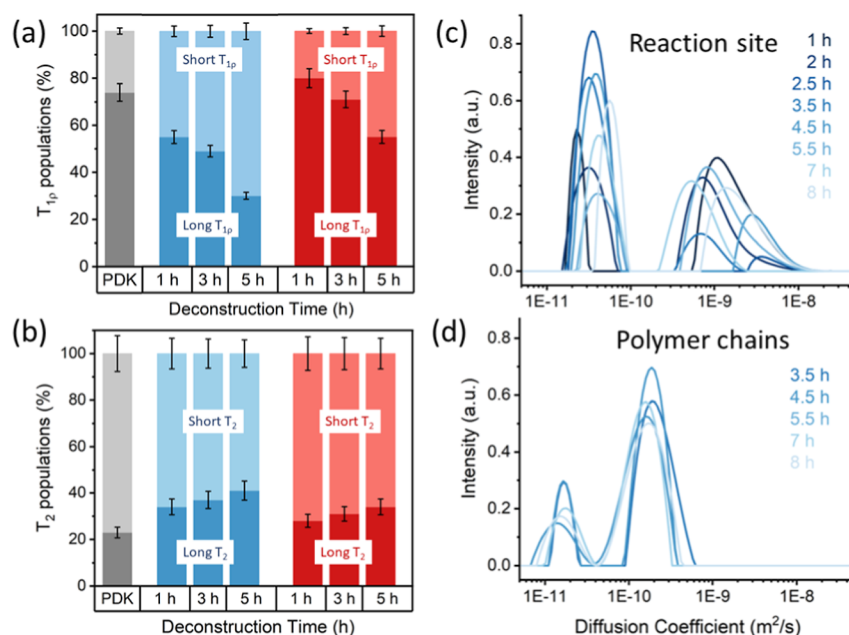
peak data and Figure S17).  $^1\text{H}$ – $^{13}\text{C}$  HSQC experiments did not show any cross peaks, suggesting an OH or NH bond.

Figure 3d displays a  $^1\text{H}$ – $^{15}\text{N}$  HSQC spectrum acquired from deconstructed PDK403 after 1 h in HBr acid dissolved in  $\text{DMSO}-d_6$  (full chemical shift range of the 2D correlation is found in Figures S18 and S19). Two cross peaks are observed:  $^1\text{H}$  at 7.8 ppm correlated to  $^{15}\text{N}$  at 32 ppm and  $^1\text{H}$  at 8 ppm correlated to  $^{15}\text{N}$  at 45 ppm. DFT calculations for suspected chemical structures of reaction intermediates were performed and are summarized in Table S1. Based upon these calculations, the first smaller NMR cross peak is assigned to a protonated primary amine;<sup>32</sup> this is further supported by the  $^{15}\text{N}$  chemical shift of T403 that resonates at 34 ppm (Figure S20). The second cross peak is assigned to the hydrogen–nitrogen bond in the proposed structure in the inset of Figure 3d (see the Supporting Information and Table S2 for detailed analysis). Intramolecular hydrogen bonding of five-membered rings in benzoxazines, reported to resonate at 8.4 ppm, leads to enhanced stability of this structure.<sup>33,34</sup> The additional oxygen–hydrogen bond maintains the structure of the intermediate state, further stabilized by a solvation shell of the counterion, resulting in enhanced stability evidenced by its presence even after 5 h of deconstruction in 5 M HBr acid. This intermediate is not a byproduct; it is present in the polymer matrix and can disappear as deconstruction progresses, enabling the elimination of the protonated amine and further monomer formation. However, its stability may lead to the inhibition of the deconstruction process. Monitoring the presence of this intermediate with solid proton NMR methods as a function of reaction time yields further insight.

Quantitative  $^1\text{H}$  high-speed MAS Hahn echo spectra (Figure 2c,d) were deconvoluted, separating the proton environments into four groups, according to their chemical shift and peak line width (Figure 4). Broad peaks, with chemical shifts originating from PDK403, were designated as “polymer”; peaks resonating at 7.3–7.6 ppm were grouped as “ $\text{NH}^+$ ”; “Intermediate/HBr” was assigned to peaks at 8–

8.5 ppm; and narrow, sharp peaks were grouped as “monomer” (Figure 4a,b). Figure 4c shows the proton populations of the designated groups for recovered PDK403 samples as a function of deconstruction time, in both 5 M HBr (blue) and 5 M  $\text{H}_2\text{SO}_4$  (red) systems (for numeric percentages, see Table S3). Protonated DKE bond ( $\text{NH}^+$ ) is evident after 1 h of reaction in acid and slowly increases with deconstruction time. Monomer formation in HBr is apparent already after 1 h, stays stable after 3 h, and greatly increases after 5 h. It is noteworthy that the intermediate group (cyclic hydrogen bond structure) is constant throughout the deconstruction process ( $\sim 10\%$ ), suggesting a stable structure. Nonetheless, after 5 h in HBr, there is still 30% of NMR intensity associated with polymer-like proton environments that have not reacted. It is important to note that this polymer-like proton signal is not pristine PDK403 situated in the inner part of the cylindrical piece, where acid cannot or has not penetrated yet (see the Materials and Methods Section for more details on sample preparation). In comparison to HBr, deconstruction in 5 M  $\text{H}_2\text{SO}_4$  yields less monomer formation throughout the process, with a constant percentage of  $-\text{NH}^+$  intermediates throughout the reaction ( $\sim 8\%$ ). This is consistent with polymer deconstruction in  $\text{H}_2\text{SO}_4$  being much slower than the deconstruction rate in HBr.

Figure 4d tracks the change in the  $^{13}\text{C}$  peak line width as a function of deconstruction time of the polymer chain environment (original NMR data in Figure 2a,b). We correlate the increase in the line width to swelling of polymer chains on the microscopic level where relaxation and/or spectral dispersion broadens lines. Macroscopic chain swelling has been reported to occur upon polymer immersion in acid,<sup>15,16</sup> leading to a distribution of  $^{13}\text{C}$  chemical environments and broadened peak line widths. An alternative rationale, given that the samples were quenched and dried, is that line broadening is associated with amorphous chain packing. As the reaction proceeds past three h, the polymer chain line width decreases, particularly for the HBr-catalyzed system. This is presumed to be associated with increased mobility of the monomer-like  $\text{CH}_x$  bonds, further supporting the



**Figure 5.** (a)  $^1H$   $T_{1\rho}$  populations and (b)  $^1H$   $T_2$  populations of PDK403 and the deconstructed polymer in 5 M HBr (blue) and 5 M  $H_2SO_4$  (red). Long relaxation is represented with dark color shade and short relaxation with lighter color shade.  $^1H$   $T_{1\rho}$  measurements were acquired with a spin-lock field of 80 kHz. Distribution of diffusion coefficients (measured with  $^1H$  PFG-NMR) analyzed with ILT as a function of PDK403 deconstruction time in 5 M DBr/ $D_2O$  (c) for reaction active site ( $-NH^+$ ) proton environment and (d) for polymer chain ( $-CH_2-$ ) proton environment.

enhanced deconstruction rate of PDK in the HBr acid medium. In comparison, broadening of the  $CH_x$  chain region is seen over the course of 5 h in  $H_2SO_4$  and presumably continues. This supports the hypothesis of slow chain swelling in  $H_2SO_4$  leading to larger pores and acid entrapment.

Considering the data presented above, we propose the following mechanistic insight (Figure S23): acidolysis of the polymer in 5 M HBr acid occurs in a swollen matrix characterized by the stress and strain of the polymer chains. Protonation of nitrogen leads to an activated DKE bond which can further form a stable reaction intermediate. The stretching and strain of swelling distorts the hydrogen bonds of the stable intermediate, resulting in further formation of the iminium bond, with subsequent water attack and monomer generation. As chain deconstruction progresses, the matrix begins to break, resulting in an unreactive conformation for the stable intermediate, which sterically hinders access to the protonated  $NH^+-C$  bond. The unreactive intermediate stays constant throughout the deconstruction process, most likely as a relatively stable untethered arm. In contrast, the kinetics of polymer acidolysis in 5 M  $H_2SO_4$  are much slower, enabling longer swelling times, and are likely to increase porosity (vide infra).

In summary, these NMR methods applied to acid deconstruction of PDK explain the chemistry shown in Figure 1a, with the formation of a protonated reaction intermediate at the amine site in PDK deconstruction in HBr that persists throughout the deconstruction process. We surmise that the reactivity of the intermediate is greatly affected by the polymer chain dynamics during matrix expansion and swelling and final chain deconstruction. This analysis prompted characterization of the motional dynamics of the residual polymers to further understand the implications of chain mobility on the reactivity of deconstruction.

**3.3. Molecular Motion and Reactivity throughout Polymer Deconstruction.** The change in line widths shown in Figure 4d reflects the relaxation rates  $R_2^*$  ( $=1/T_2^*$ ) and thus is influenced by molecular motion with narrow lines (longer  $T_2^*$ ) associated with increased mobility.<sup>35</sup> These line width observations prompted us to use measurements of spin–lattice relaxation in the rotating frame ( $R_{1\rho}$ ,  $=1/T_{1\rho}$ ) to further analyze this system because  $R_{1\rho}$  is a sensitive probe of molecular motion on the time scale of ms–s (corresponding

to spin-lock frequencies of a few Hz to a few kHz).<sup>36</sup> We note that for longer  $T_2^*$  and shorter  $T_{1\rho}$  relaxation to be associated with increased mobility, one has to be on the correct side of the  $\tau_c\omega_0$  minimum, with increased motion resulting in shorter correlation times.<sup>37</sup> Finally, we discern molecular motion by measuring macroscopic displacement of nuclear spins by PFG diffusion measurements (PFG-NMR); in our case, this method probes the longer length scale motion of chemical moieties. Here, the derived “self-diffusion coefficient”  $D$  (dimensions of  $m^2 s^{-1}$ ) quantitates the macroscopic motion where larger  $D$  corresponds to faster motion. We examine all of these measurements for the HBr and  $H_2SO_4$  deconstruction reactions.

Figure 5a shows our analysis of  $^1H$   $T_{1\rho}$  measurements of the polymer samples during the first 5 h of deconstruction (see Table S4 for nominal results); a simplified analysis of these rates produces biexponential decays shown as the ratio between the populations of slow and fast  $^1H$   $T_{1\rho}$  relaxation times. From the point of view of polymer motion and  $T_{1\rho}$ , pristine PDK403 consists of two dynamic regimes, 26% with more rapid relaxation ( $530 \mu s$ ), corresponding to faster motion, and 74% with slower relaxation (2.5 ms), corresponding to slower motion. As deconstruction proceeds in HBr acid, the harvested residual polymer shows an increasing fraction of the region associated with short  $T_{1\rho}$  values, i.e., faster relaxation rates and more rapid motion. We submit that these values are consistent with monomer formation, leading to the presence of fast-moving smaller chains. Further evidence of the fast motion regime can be seen in Figure 5b, portraying the increase in the  $^1H$   $T_2$  relaxation as deconstruction proceeds (nominal  $T_2$  relaxation results can be found in Table S5).

The ratio of slow/fast motion as a function of deconstruction time agrees with the fractional line shape analysis portrayal shown in Figures 4c and S24. A similar trend is observed for the relative segments of fast and slow  $^1H$   $T_{1\rho}$  relaxation times of deconstructed samples in 5 M  $H_2SO_4$ , though the increase in population of faster moving polymer chains is more gradual over time due to slower deconstruction kinetics in this system. However, two distinct domains of motion are clearly observed for all deconstructed samples, further supporting the dynamic morphological heterogeneity of the deconstruction process. It should be noted that  $^1H$   $T_{1\rho}$  relaxation times presented here, equivalent to local motion in the samples, are

averaged over the entire sample volume without chemical specificity. Figure S25 shows that a normalized comparison of line widths and relaxation rates for the HBr and H<sub>2</sub>SO<sub>4</sub> residual polymers reveals clear trends for increased regions of polymer mobility in the residual products.

Self-diffusion measurements in situ of the acid deconstruction process are shown in Figure 5c,d. Measurements were performed over a course of ~8 h of deconstruction, utilizing multiexponential ILT<sup>20</sup> to analyze the attenuation of the <sup>1</sup>H PFG-NMR signal, resulting in a distribution of the translational self-diffusion coefficients (*D*) for the specific proton chemical environments. Figure 5c,d shows the distributions of *D* for the reaction site (protonated amine group, integration of peak at 7.5–8.5 ppm) and the protons in CH<sub>2</sub> polymer chains (integration of peak at 0.8–1.5 ppm) as a function of reaction time in DBr/D<sub>2</sub>O, respectively. Both functional groups exhibit bimodal distributions of self-diffusion coefficients *D*.

The bimodal distributions for polymer chain diffusion (Figure 5d) can be parsed into two domains of motion, with average diffusion coefficients of  $1.7 \times 10^{-10} \text{ m}^2 \text{ s}^{-1}$  and  $1.6 \times 10^{-11} \text{ m}^2 \text{ s}^{-1}$ . We assign the slower motion to semioriented, unreacted polymer chains that are largely unaffected by the reaction time. The larger self-diffusion coefficient can be assigned to polymer chains that are “splaying” as the reaction proceeds, hence presenting increased local mobility. Further assessment of the mobility of a swelled polymer matrix was performed by monitoring PDK403 in different solvents and can be found in Table S6. Concentrated acid shows better polymer swelling capabilities than pure D<sub>2</sub>O and consequently faster self-diffusion but inferior to swelling properties of an organic solvent like chloroform.

The bimodal distribution of diffusion coefficients for the reaction active (–NH<sup>+</sup>) proton site, seen in Figure 5c, also presents two regions of local motion, where the slower component likely arises from the strong tethering effect of the polymer backbone. Indeed, the distribution of this slower *D* is the average of the slow and moderate polymer chain motions, as seen in Figure 5d. The faster self-diffusion coefficient is on the same order of magnitude as H<sub>3</sub>O<sup>+</sup> molecular diffusion<sup>15</sup> measured during deconstruction of DKE. This enhanced mobility results from increased movement of protons at the reaction site that undergo fragmentation and exhibit escalated free motion in the acid solution (further discussion of the ILT analysis and ratio of the fast and slow motions as a function of deconstruction time can be found in the Supporting Information and Figures S26–S29).

It should be noted that the deconstruction time dependence of the diffusion coefficients is not straightforward and does not show a clear increase or decrease in *D* in time. The nonlinearity of the molecular diffusivity and the complexity of the deconstruction process result from the intercalation of different factors affecting the deconstruction, such as swelling, diffusion, and reaction. Correlation of polymer deconstruction with fractal kinetics has been reported recently,<sup>16</sup> where fractal-based equations are employed to parametrize rate laws. Nonetheless, the diverse and heterogeneous essence of polymer motion throughout the deconstruction process is clear. In our analyses, the slow diffusive motion of the rigid polymer chains greatly affects the motion of the reaction site, at times being the dominant motion measured, while the fast mobility of the reaction site steers the hydrolysis forward. These results provide experimental evidence supporting a multipathway deconstruction mechanism in HBr, shedding light on the importance of local chain dynamics and its control over the reactivity and stability of the formed intermediate.

## 4. CONCLUSIONS

Heterogeneous deconstruction of a model elastomer featuring acid-cleavable DKE bonds is presented in 5 M HBr and H<sub>2</sub>SO<sub>4</sub> acid solutions, with the advancement and application of magnetic resonance methodologies offering insights.

Polymer deconstruction is complex and not uniform: different regions of the polymer begin to react, becoming more susceptible to acid penetration, while other regions remain unaffected by contact with acid. Although monomer

formation is evident even at early stages of the deconstruction process, remnants of the polymer can be seen even after 5 h in both HBr- and H<sub>2</sub>SO<sub>4</sub>-concentrated acid systems.

On the molecular level, it is clear that deconstruction in HBr is faster than that in H<sub>2</sub>SO<sub>4</sub> containing aqueous media. We show clear evidence of differing deconstruction mechanisms in these acids. The chaotropic nature of HBr facilitates the high mobility of the reaction site, prompting formation of a rather stable intermediate and necessitating an additional energy barrier for completion of the reaction. Stretching and strain during polymer matrix swelling promotes the reactive conformation of the intermediate, resulting in monomer formation. After chain deconstruction occurs, the intermediate remains in its stationary form. The diffusivity behavior of the reaction site, strongly linked to the moderate-to-slow kinetics of the polymer chains, further demonstrates this complex polymer deconstruction process. In contrast, slow deconstruction kinetics of the polymer follows from slower swelling in H<sub>2</sub>SO<sub>4</sub>, enabling emerging porosity of the polymer and acid entrapment within.

The ability to understand reaction mechanisms allows the refinement of deconstruction conditions. We submit that enhanced local chain mobility is critical to ensure reactive configurations and fast and clean polymer deconstruction; such local mobilities can be controlled with material design, e.g., by the addition of heteroatoms in the polymer backbone.

We conclude that NMR methodologies provide molecular insight into polymer deconstruction by relating local structure to molecular mobility, thereby adding further guidance to the planning and production of future circular materials.

## ■ ASSOCIATED CONTENT

### Data Availability Statement

All data needed to evaluate the conclusions are present in the paper and/or the Supporting Information, as well as in the Dryad Repository at doi:10.5061/dryad.n8pk0p34g.

### SI Supporting Information

The Supporting Information is available free of charge at <https://pubs.acs.org/doi/10.1021/acs.macromol.4c02353>.

<sup>1</sup>H NMR spectra of PDK403, monomers T403 and TK, and degraded polymer in various deuterated solvents; photo of recovered polymer after acid treatment; comparison of in situ and ex-situ testing; <sup>1</sup>H ssNMR spectrum of TK powder, PDK403, PDK3000, and PDK5000; <sup>1</sup>H spectra of degraded polymers after base treatment; <sup>1</sup>H variable temperature trials of the recovered polymer; NMR 2D correlations, <sup>1</sup>H–<sup>1</sup>H COSY, <sup>1</sup>H–<sup>1</sup>H NOESY for recovered PDK403 and recovered DKE; <sup>1</sup>H–<sup>15</sup>N HSQC; <sup>1</sup>H selective NOESY of the recovered polymer; <sup>15</sup>N spectrum of PDK403 and T403; molecular structure of the proposed intermediate; deconvolution of <sup>1</sup>H ssNMR spectra of the recovered polymer; energy surface of different deconstruction pathways; ILT analysis and discussion for polymer diffusion in D<sub>2</sub>O, CDCl<sub>3</sub>, DBr, and D<sub>2</sub>SO<sub>4</sub>; summary of proposed structure and DFT calculations; <sup>1</sup>H–<sup>15</sup>N HSQC cross peaks; <sup>1</sup>H ssNMR integration intensities; *T*<sub>1ρ</sub> and *T*<sub>2</sub> relaxation data; and average diffusion coefficients (PDF)

## AUTHOR INFORMATION

### Corresponding Authors

**Shira Haber** – *Materials Sciences Division, Lawrence Berkeley National Laboratory, Berkeley, California 94720, United States*; Present Address: Department of Chemistry, Ben-Gurion University of the Negev, Beer-Sheva, 84105, Israel; [orcid.org/0009-0003-6916-4871](https://orcid.org/0009-0003-6916-4871); Email: [habersh@post.bgu.ac.il](mailto:habersh@post.bgu.ac.il)

**Jeffrey A. Reimer** – *Materials Sciences Division, Lawrence Berkeley National Laboratory, Berkeley, California 94720, United States*; Department of Chemical and Biomolecular Engineering, University of California, California 94720, United States; Email: [reimer@berkeley.edu](mailto:reimer@berkeley.edu)

### Authors

**Julia Im** – *Department of Chemical and Biomolecular Engineering, University of California, California 94720, United States*; [orcid.org/0000-0002-6633-2513](https://orcid.org/0000-0002-6633-2513)

**Mutian Hua** – *Materials Sciences Division, Lawrence Berkeley National Laboratory, Berkeley, California 94720, United States*; Present Address: School of Environmental and Forest Sciences, University of Washington, Seattle, WA, 98195, United States.

**Alexander R. Epstein** – *Department of Materials Sciences and Engineering, University of California, California 94720, United States*; Present Address: Yusuf Hamied Department of Chemistry, University of Cambridge, Lensfield Road, Cambridge, CB2 1EW, UK.

**Sophia N. Fricke** – *Department of Chemical and Biomolecular Engineering, University of California, California 94720, United States*; [orcid.org/0000-0002-0183-466X](https://orcid.org/0000-0002-0183-466X)

**Raynald Giovine** – *Pines Magnetic Resonance Center, Core NMR Facility, College of Chemistry, University of California, Berkeley, California 94720, United States*; [orcid.org/0000-0002-7208-6929](https://orcid.org/0000-0002-7208-6929)

**Hasan Celik** – *Pines Magnetic Resonance Center, Core NMR Facility, College of Chemistry, University of California, Berkeley, California 94720, United States*

**Kristin A. Persson** – *Materials Sciences Division, Lawrence Berkeley National Laboratory, Berkeley, California 94720, United States*; Department of Chemical and Biomolecular Engineering, University of California, California 94720, United States; The Molecular Foundry, Lawrence Berkeley National Laboratory, Berkeley, California 94720, United States

**Brett A. Helms** – *Materials Sciences Division, Lawrence Berkeley National Laboratory, Berkeley, California 94720, United States*; The Molecular Foundry, Lawrence Berkeley National Laboratory, Berkeley, California 94720, United States; [orcid.org/0000-0003-3925-4174](https://orcid.org/0000-0003-3925-4174)

Complete contact information is available at:

<https://pubs.acs.org/10.1021/acs.macromol.4c02353>

### Author Contributions

The CRediT author contributions are as follows: S.H., J.A.R., S.N.F., M.H., and B.A.H. contributed to the conceptualization of the project. S.H. and J.A.R. contributed to the design of the project. M.H. contributed to the design of PDK elastomers and DKE materials. A.R.E. performed all DFT simulations. NMR characterization and analysis was performed by S.H. and J.I. ILT analysis for PFG-NMR was performed by J.I. Further NMR methodology and development was performed by S.H., R.G., and H.C. S.H., J.I., A.R.E., S.N.F., and M.H. contributed

to visualization. S.H. wrote the original draft. J.I. wrote the PFG-NMR discussion with S.H. supervision. All authors contributed to the final draft and editing. J.A.R., B.A.H., and K.A.P. supervised research, provided project administration, and acquired funding.

### Funding

This work was funded by the U.S. Department of Energy, Office of Science, Office of Basic Energy Sciences, Materials Sciences and Engineering Division, under contract no. DE-AC02-05-CH11231, Unlocking Chemical Circularity in Recycling by Controlling Polymer Reactivity across Scales program CUP-LBL-Helms. Work at the Molecular Foundry, polymer and small molecule synthesis and characterization, was done and supported by the Office of Science, Office of Basic Energy Sciences, of the U.S. Department of Energy under contract no. DE-AC02-05CH11231. A.R.E. was supported by the National Science Foundation Graduate Research Fellowship under grant no. DGE 1752814.

### Notes

The authors declare the following competing financial interest(s): The authors declare the following competing interests: B.A.H. is an inventor on the US provisional patent application 62/587,148 submitted by Lawrence Berkeley National Laboratory that covers PDKs, as well as aspects of their use and recovery. A.R.E., K.A.P., and B.A.H. are inventors on the US provisional patent application 63/390,962 submitted by Lawrence Berkeley National Laboratory that covers elastomeric PDKs, as well as aspects of their use and recovery. B.A.H. has a financial interest in Cyklos Materials and Sepion Technologies.

## ACKNOWLEDGMENTS

We thank Pines Magnetic Resonance Center's Core NMR Facility (PMRC Core) for spectroscopic resources used in this study. The instrument used in this work for  $^1\text{H}$  PFG-NMR measurements and variable-temperature  $^1\text{H}$  NMR measurements was supported by the National Science Foundation under grant no. 2018784. The instrument used for acquiring  $^{15}\text{N}$  measurement of the T403 monomer and selective  $^1\text{H}$  NOESY measurements was supported in part by NIH S10OD024998. This research used the Savio computational cluster resource provided by the Berkeley Research Computing program at the University of California, Berkeley (supported by the UC Berkeley Chancellor, Vice Chancellor for Research, and Chief Information Officer). We thank Norman Su and Huntsman Corp., for providing the triamine monomers used in the study. S.N.F. gratefully acknowledges support as a Pines Magnetic Resonance Center Postdoctoral Fellow.

## REFERENCES

- (1) Helms, B. A. Polydiketoamines for a Circular Plastics Economy. *Acc. Chem. Res.* **2022**, *55* (19), 2753–2765.
- (2) Häußler, M.; Eck, M.; Rothauer, D.; Mecking, S. Closed-Loop Recycling of Polyethylene-like Materials. *Nature* **2021**, *590* (7846), 423–427.
- (3) Abel, B. A.; Snyder, R. L.; Coates, G. W. Chemically Recyclable Thermoplastics from Reversible-Deactivation Polymerization of Cyclic Acetals. *Science* (1979) **2021**, *373*, 783–789.
- (4) Coates, G. W.; Getzler, Y. D. Y. L. Chemical Recycling to Monomer for an Ideal, Circular Polymer Economy. *Nat. Res. Mater.* **2020**, *5*, 501–516.

## Supplementary Materials for:

### **Mechanisms Underpinning Heterogeneous Deconstruction of Circular Polymers: Insight from Magnetic Resonance Methodologies**

Shira Haber,<sup>\*[a]</sup> Julia Im,<sup>[b]</sup> Mutian Hua,<sup>[a],[c]</sup> Alexander R. Epstein,<sup>[d]</sup> Sophia N. Fricke,<sup>[b]</sup> Raynald Giovine,<sup>[e]</sup> Hasan Celik,<sup>[e]</sup> Kristin A. Persson,<sup>[a],[b],[f]</sup> Brett A. Helms,<sup>[a],[f]</sup> and Jeffrey A. Reimer<sup>\*[a],[b]</sup>

[a] Dr. S. Haber, Dr. M. Hua, Prof. K.A. Persson, Dr. B.A. Helms, Prof. J.A. Reimer  
Materials Sciences Division,  
Lawrence Berkeley National Laboratory,  
Berkeley, CA 94720 USA.  
Email: habersh@post.bgu.ac.il  
Email: reimer@berkeley.edu

[b] J. Im, Dr. S.N. Fricke, Prof. K.A. Persson, Prof. J.A. Reimer  
Department of Chemical and Biomolecular Engineering,  
University of California, Berkeley,  
Berkeley, CA 94720 USA.

[c] Present address:  
Dr. M. Hua  
School of Environmental and Forest Sciences,  
University of Washington,  
Seattle, WA, 98195

[d] Dr. A.R. Epstein  
Department of Materials Sciences and Engineering,  
University of California, Berkeley,  
Berkeley, CA 94720 USA.  
Present address:  
Yusuf Hamied Department of Chemistry,  
University of Cambridge,  
Lensfield Road, Cambridge, CB2 1EW UK.

[e] Dr. R. Giovine, Dr. H. Celik  
Pines Magnetic Resonance Center, Core NMR Facility, College of Chemistry,  
University of California, Berkeley,  
Berkeley, CA, 94720 USA.

[f] Prof. K.A Persson, Dr. B.A. Helms  
The Molecular Foundry,  
Lawrence Berkeley National Laboratory,  
Berkeley, CA 94720 USA.

\*corresponding authors

**This file contains:**

Figure S1 to S29

Tables S1 to S6

References

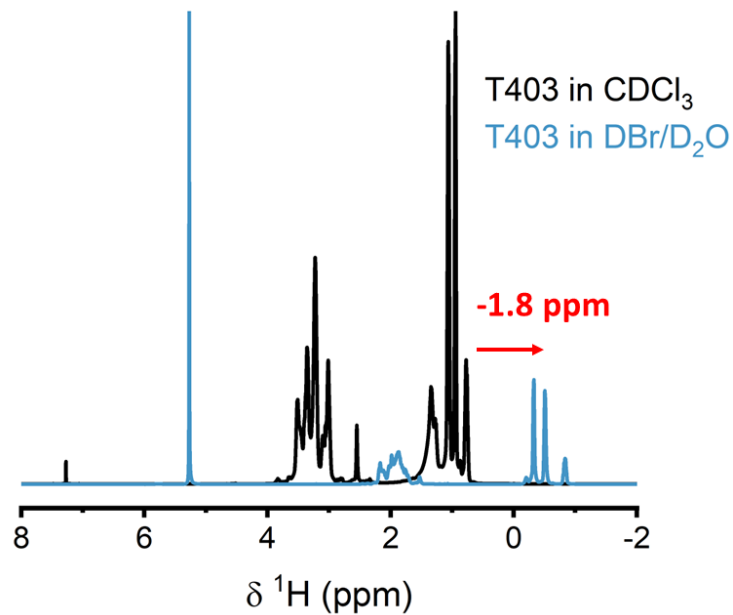


**Figure S1.**  $^1\text{H}$  NMR spectra of triamine crosslinker, T403, dissolved in  $\text{CDCl}_3$  (black) and dissolved in 5 M  $\text{DBr} / \text{D}_2\text{O}$  (blue) acquired at 11.7 T. A shift to lower frequency (upfield) of 1.8 ppm is seen due to the high concentration of acid solution in the sample.

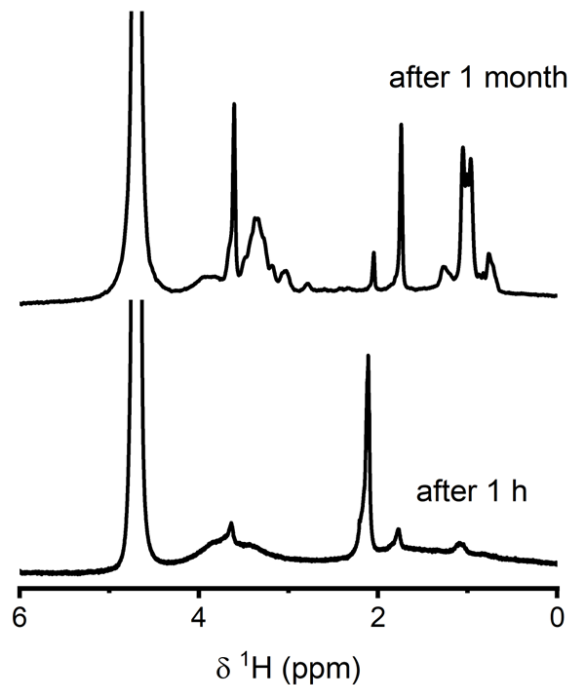


**Figure S2.**  $^1\text{H}$  NMR spectra of a slice of PDK403 acquired after 1 h in  $\text{D}_2\text{O}$  (bottom spectrum) and acquired again after immersion for 1 month in  $\text{D}_2\text{O}$  (top spectrum) acquired at 11.7 T. Minimal proton signal is seen after 1 h immersion due to the polymer's limited solubility in water. After 1 month, the proton signal grows in intensity and spectral resolution increases enabling separation and identification of different environments. This results from water penetration into the polymer chains and formation of a solvation shell.

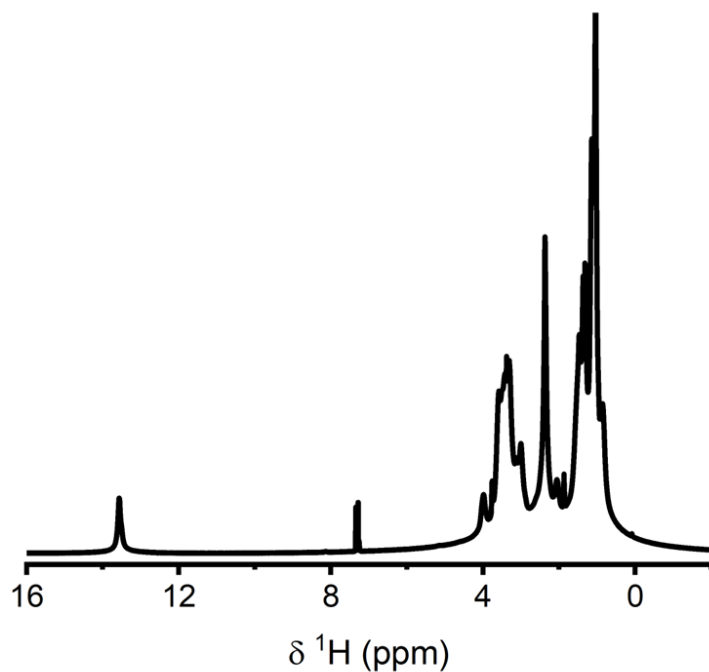


**Figure S3.**  $^1\text{H}$  spectrum of PDK403 acquired after immersion for 5 h in  $\text{CDCl}_3$ . Immediately upon polymer immersion in chloroform, proton signal could not be acquired due to minimal solubility. After 5 h, swelling of the polymer occurs, with chloroform solvent penetrating into the inner chains, requiring addition of more  $\text{CDCl}_3$  to the NMR tube before measurement. Spectrum was acquired at 11.7 T.

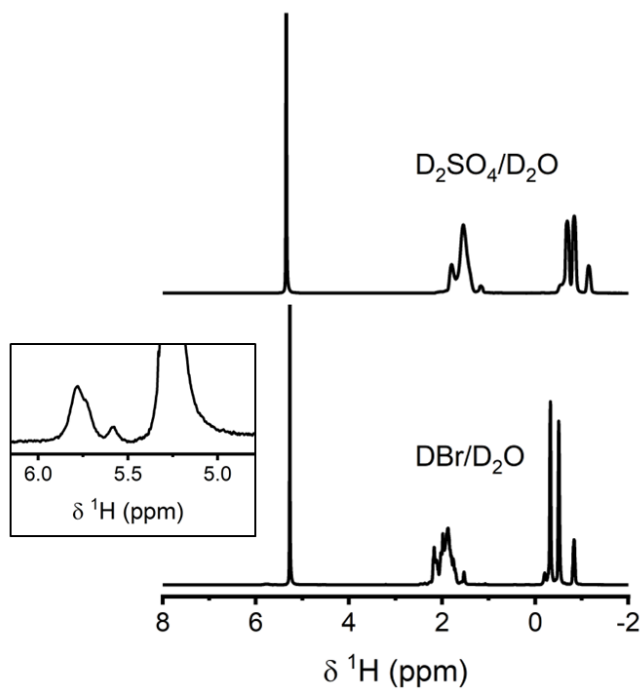


**Figure S4.** <sup>1</sup>H spectra of T403 in 5 M DBr/D<sub>2</sub>O (bottom spectrum) and in 5 M D<sub>2</sub>SO<sub>4</sub>/D<sub>2</sub>O (top spectrum). Chemical shift axis is shifted due to high acid concentration. Peak resolution of monomer in DBr acid is higher than D<sub>2</sub>SO<sub>4</sub> due to the chaotropic ion vs the kosmotropic ion properties of the anions in the solution, affecting the solvation and polymer–water interactions. In addition, a new peak at 5.8 ppm can be seen in the sample of T403 in DBr, assigned to the protonated amine environment. Spectra were acquired at 11.7 T.

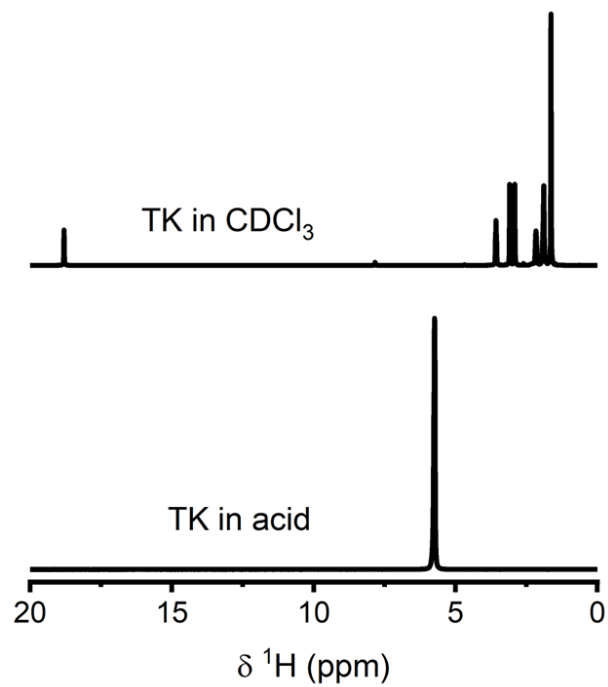


**Figure S5.** <sup>1</sup>H spectra of TK monomer in 5 M DCl / D<sub>2</sub>O (bottom) and in CDCl<sub>3</sub> (top). TK is not soluble in acid, floats or precipitates; thus a proton signal cannot be acquired. Spectra were acquired at 11.7 T.



**Figure S6.** Photo of recovered PDK403 after 1 h in 5 M HBr and overnight drying. In general, a cylindrical piece of PDK403 was placed in a vial with excess 5 M acid solution and a magnetic stir bar. After the desired amount of time for deconstruction, the solid polymer was filtered, washed with acid to remove undesired residual eliminated triamines, and further washed with water. The recovered polymer was dried overnight at 60 °C under vacuum conditions, leading to a yellow, swelled hollow network. The outer matrix of the polymer, which came in contact with the acid and underwent deconstruction, is porous and brittle. This part of the recovered polymer was ground up and placed in the NMR rotors for measurements. The inner part of the cylindrical polymer remained undegraded due to lack of acid penetration, showing the same density and consistency as the original polymer. This part was not tested.

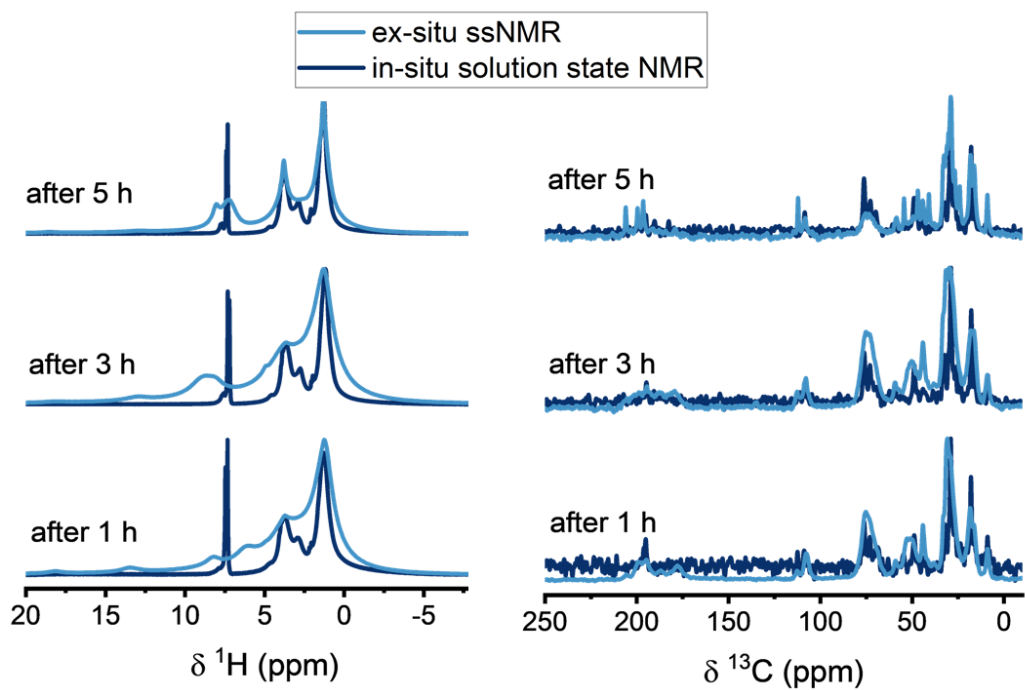


**Figure S7.** Comparison of  $^1\text{H}$  (left) and  $^{13}\text{C}$  (right) NMR spectra acquired with in situ conditions and *ex-situ* conditions of PDK403 deconstruction in 5 M HBr (see Methods and Materials section for more details). Solution-state NMR measurements were acquired at 11.7 T. ssNMR samples were prepared and measured between 2–3 times to ensure repeatability at 9.4 T.

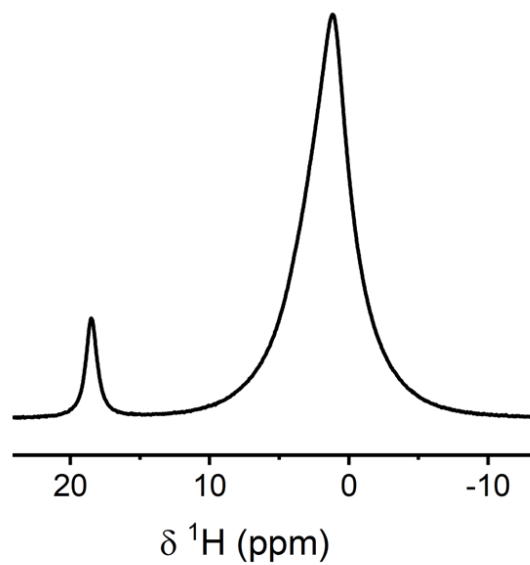


**Figure S8.**  $^1\text{H}$  Hahn echo measurement of TK powder. A strong peak at 18 ppm can be seen, coming from the proton of the enol group. Spectrum was acquired at 9.4 T.

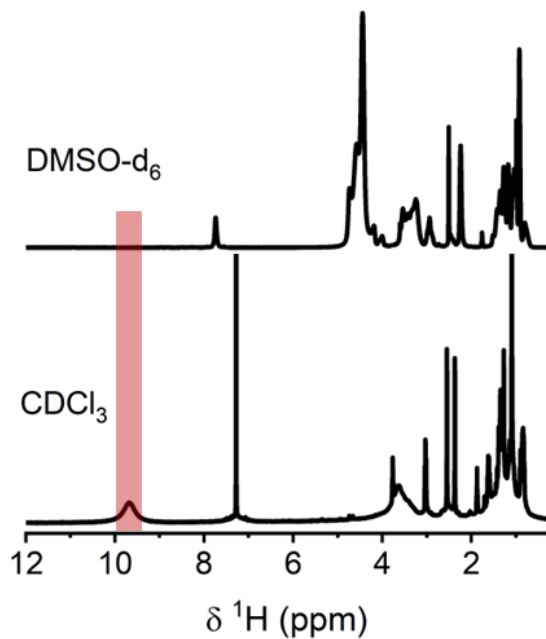


**Figure S9.** Comparison of <sup>1</sup>H spectra of degraded PDK403 after 5 h in 5 M H<sub>2</sub>SO<sub>4</sub>. The solid sample was filtered, washed with acid, washed with water, and dried overnight under vacuum at 60 °C. Recovered outer layers of polymer were ground up and dissolved in CDCl<sub>3</sub> (bottom) and in DMSO-*d*<sub>6</sub> (top). A peak at 9.7 ppm can be seen in deuterated chloroform solvent but not in deuterated DMSO. This proves the existence of hydrogen bonds (fast exchange with the deuterium of DMSO-*d*<sub>6</sub> on the NMR timescale results in lack of signal). Spectra were acquired at 11.7 T.

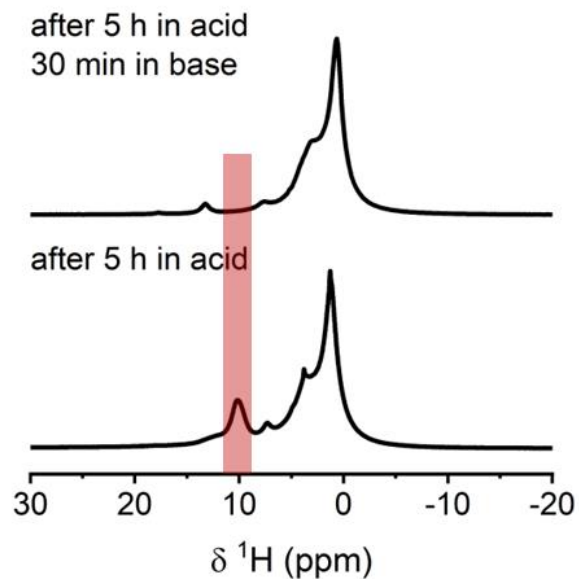


**Figure S10.**  $^1\text{H}$  spectra of recovered polymer after 5 h in 5 M  $\text{H}_2\text{SO}_4$  (bottom) and after additional immersion in 5 M  $\text{NaOH}$  solution (top). Both solid samples were filtered, washed with acid/base, with water and dried under vacuum at 60 °C. Outer layers of recovered polymer were ground up and packed into rotor for measurements. Environment at 10 ppm cannot be seen after base treatment, proving the acidity of this proton environment. Spectra were acquired at 9.4 T.

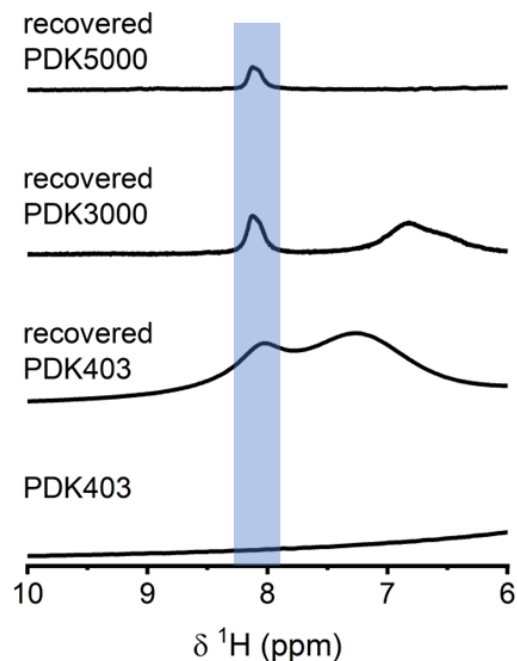


**Figure S11.** To further investigate the intermediate proton environment resonating at 8–9 ppm, additional formulations of PDK were degraded in 5 M HBr acid, differing in the length of the triamine polypropylene crosslinker monomer used in polymer synthesis, leading to increased molar mass of  $3000 \text{ g mol}^{-1}$  and  $5000 \text{ g mol}^{-1}$ . Comparative  $^1\text{H}$  Hahn echo spectra of recovered polymers (PDK403, PDK3000, and PDK5000) after 1 h in 5 M HBr solution, compared to pristine PDK403 is shown above. A distinct peak at  $\sim 8$  ppm is evidenced for all degraded polymer samples, regardless of their molecular weight, signifying that cross-linkage density has minimal effect on the evolution of this intermediate environment. Spectra were acquired at 9.4 T.

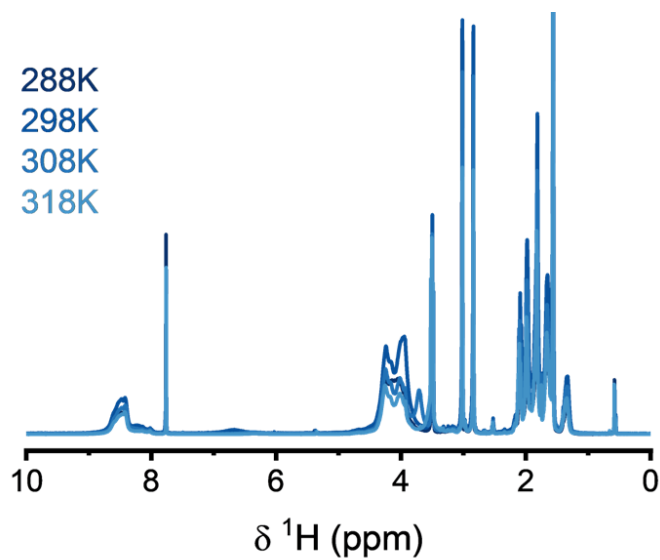


**Figure S12.** Variable temperature <sup>1</sup>H measurements of recovered polymer after 1 hour in 5 M HBr. Solid sample was filtered, washed with acid, then with water, dried under vacuum at 60°C, and dissolved in CDCl<sub>3</sub>. Chemical shift of the environment resonating at 8 ppm stays constant with temperature change. Spectra were acquired at 9.4 T.

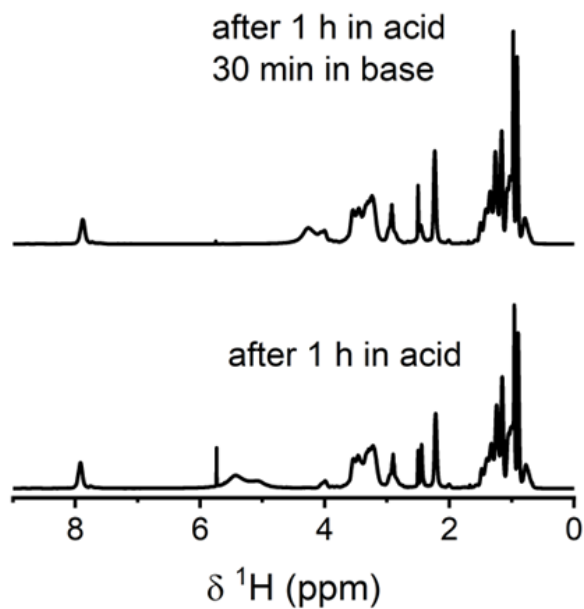


**Figure S13.** <sup>1</sup>H spectra of recovered polymer after 1 h in 5 M HBr (bottom) and after immersion in 5 M NaOH solution (top). Both solid samples were filtered, washed with acid/base, followed by washing with water, dried under vacuum at 60 °C, then dissolved in CDCl<sub>3</sub>. Environment at 8 ppm remains intact after base treatment. Spectra were acquired at 11.7 T.

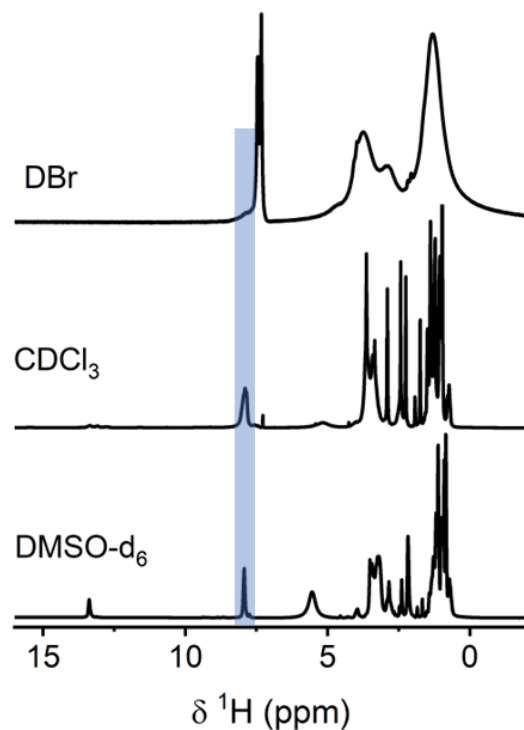


**Figure S14.** Sample dissolution in deuterated solvents was enabled due to the increased solubility of the deconstructed PDK403. Comparison of  $^1\text{H}$  spectra of degraded PDK403 after 1 h: in 5 M DBr /  $\text{D}_2\text{O}$  (top), solid sample dissolved in  $\text{CDCl}_3$  (middle) and in  $\text{DMSO-}d_6$  (bottom) after 1 hour deconstruction in 5 M HBr, filtered, washed with acid, then with water and vacuum dried at 60 °C. A peak at  $\sim 8$  ppm can be seen. The change in peak intensity and linewidth, as a function of deuterated solvent, indicate the presence of hydrogen bonds, N-H or O-H. Spectra were acquired at 11.7 T.

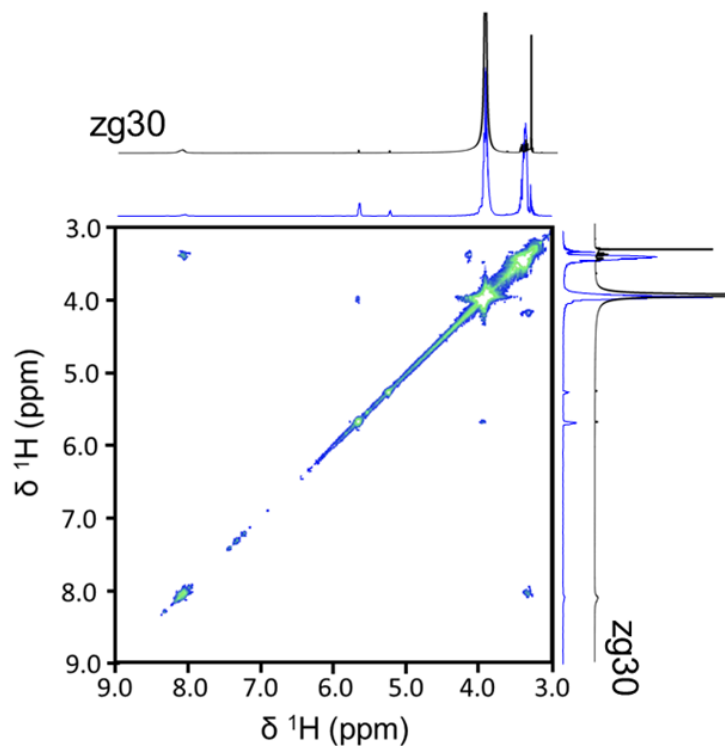


**Figure S15.**  $^1\text{H}$ - $^1\text{H}$  Correlated Spectroscopy (COSY) measurement of recovered DKE after 1 h in 5 M HCl. An aliquot of sample was extracted, and mixed with  $\text{DMSO-}d_6$ . A cross peak is seen, attributed to the proton adjacent to the ether,  $\text{CH}_2\text{-O-}$ , resonating at 3.4 ppm correlating with  $^1\text{H}$  at 8 ppm. The lack of a cross peak between the proton of the 8 ppm environment and the proton adjacent to the nitrogen ( $\text{-N-CH}$ ) is explained by the fact that these protons are on planes with a dihedral angle of  $72^\circ$  leading to minimal orbital overlap and low coupling.<sup>1</sup> Spectrum was acquired at 11.7 T.

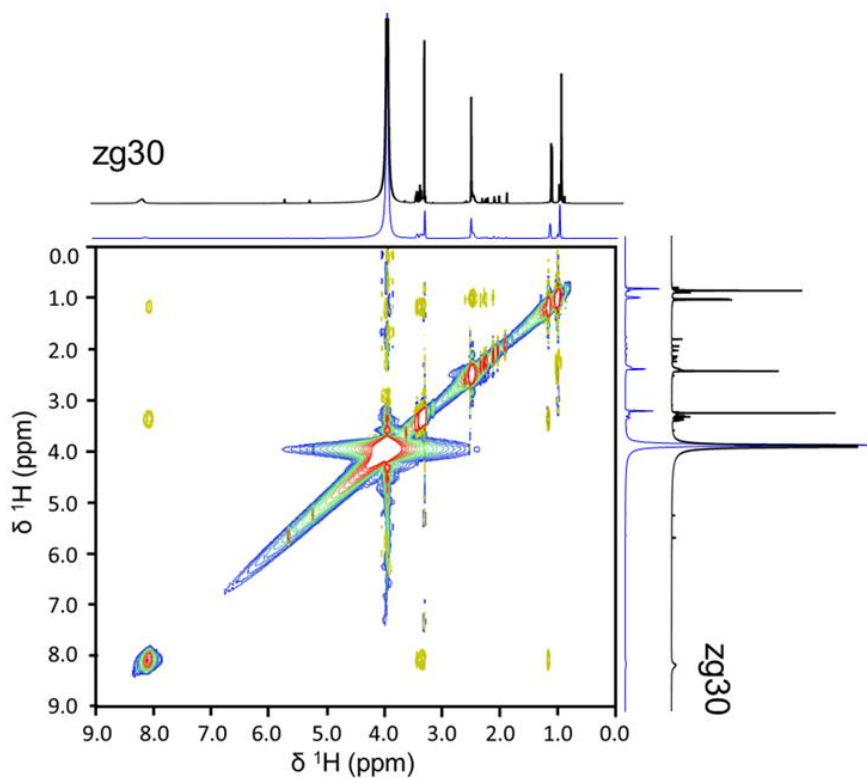


**Figure S16.**  $^1\text{H}$ - $^1\text{H}$  Nuclear Overhauser Effect Spectroscopy (NOESY) measurement of recovered DKE after 1 h in 5 M HCl. An aliquot of sample was extracted, and mixed with  $\text{DMSO-}d_6$ . Two cross peaks with 8 ppm are evidenced: the first correlates with 3.4 ppm, assigned to  $\text{CH}_2\text{-O-}$  site, and can be seen in  $^1\text{H}$ - $^1\text{H}$  COSY in Figure S15 since they are geminal protons. The second cross peak correlates  $^1\text{H}$  at 8 ppm with  $^1\text{H}$  at 1.2 ppm, assigned to the methylene chain,  $-\text{CH}_2-$  group. The negative signal of the cross peaks, in comparison to the positive signal of the diagonal peak, results from the small molecules in the sample.<sup>2</sup> In small molecules, NOESY cross peaks exhibit an opposite sign to the diagonal peaks, while measurements of large molecules, both cross and diagonal peaks share the same sign. Spectrum was acquired at 11.7 T.

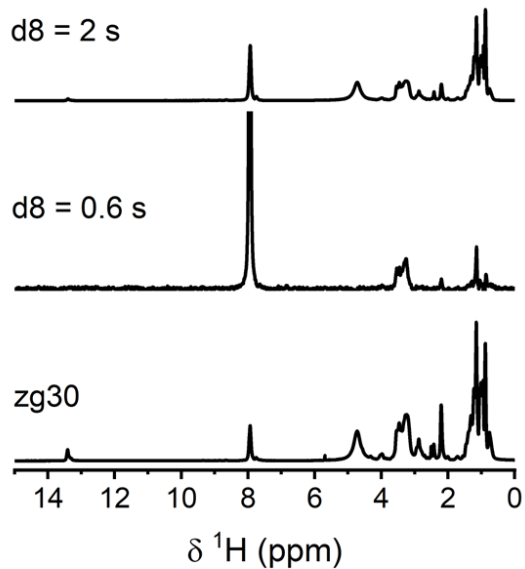


**Figure S17.**  $^1\text{H}$  selective NOESY (compared with zg30 spectrum, bottom spectrum) of recovered polymer after 1 h in 5 M HBr. Solid sample was filtered, washed with acid, then with water, dried under vacuum at 60 °C and dissolved in  $\text{DMSO-}d_6$ . Transmitter frequency ( $\omega_{\text{1p}}$ ) was focused on 8 ppm to follow specific correlations. Increasing the mixing times (d8) leads to additional correlations of the proton resonating at 8 ppm with the rest of the proton environments of the sample. Spectra were acquired at 14.1 T.

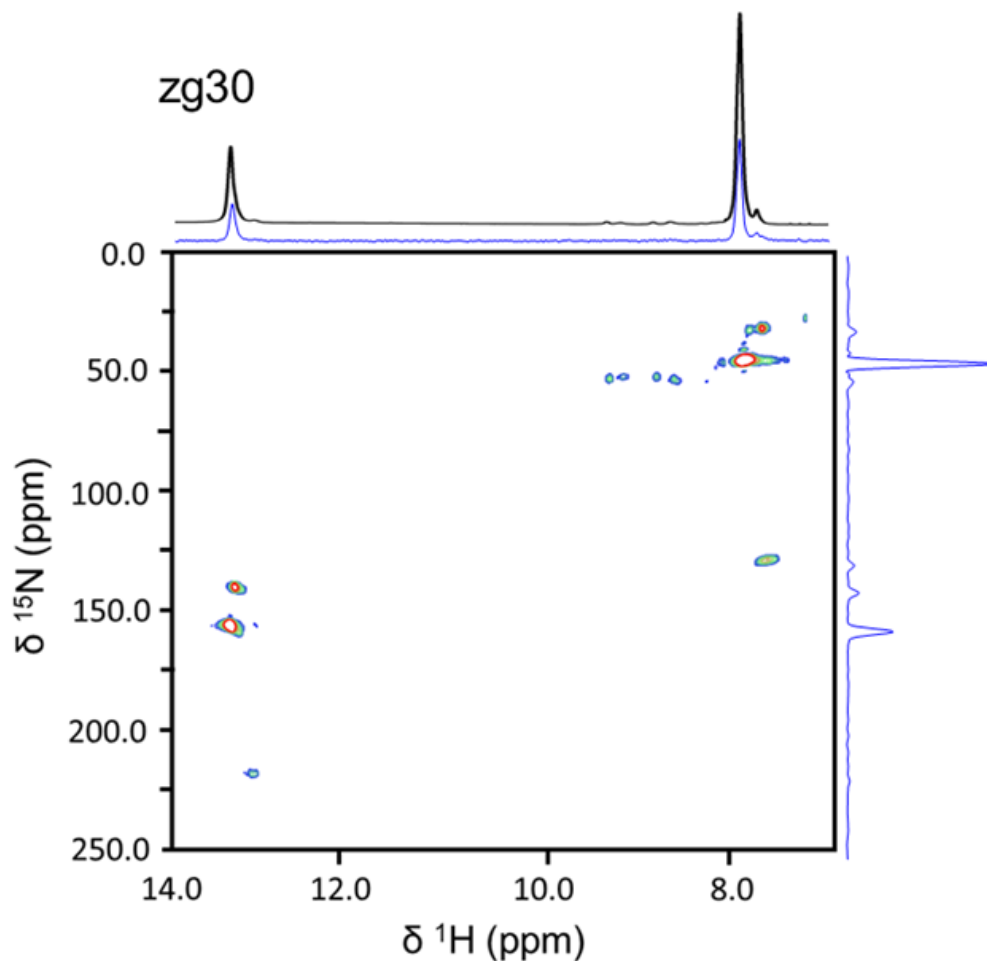


**Figure S18.**  $^1\text{H}$ - $^{15}\text{N}$  Heteronuclear Single Quantum Coherence (HSQC) measurement of recovered polymer after 1 h in 5 M HBr. Solid sample was filtered, washed with acid, then with water, dried under vacuum at 60 °C and dissolved in  $\text{DMSO-}d_6$ . Cross peak validity and their chemical shifts were verified by running experiment with different transmitter frequency offsets ( $\text{O}_{2p}$ ). Spectrum was acquired at 11.7 T.

It is clear that the recovered polymer consists of a mixture of various intermediates at different stages of deconstruction. Nitrogen environments can be separated into two groups according to their chemical shifts: secondary amines resonating at 30–60 ppm and another nitrogen group resonating at 120–240 ppm. Cross peaks are summarized in Table S2.

The proton shift of secondary protonated amines has been reported at 8–9 ppm<sup>3</sup> and the  $^{15}\text{N}$  chemical shift corresponds to a secondary ammonium,<sup>4</sup> single bonded to carbon (see Table S1). Simulating an intramolecular hydrogen bond, between the ionized amine and the ether oxygen

in the polymer leads to proximity between the ketone oxygen and the additional proton that is bonded to the nitrogen (see Figure S21 for calculated hydrogen bond lengths). This additional oxygen-hydrogen bond maintains the structure of the intermediate state,<sup>5,6</sup> further stabilized by a solvation shell of the counter ion, resulting in enhanced stability and residues of this state even after 5 h of deconstruction in 5 M HBr acid, with mixing. Integration of <sup>1</sup>H spectrum of the degraded DKE after 1 h in acid indicates that two protons are overlapping at 8 ppm (Figure S22).

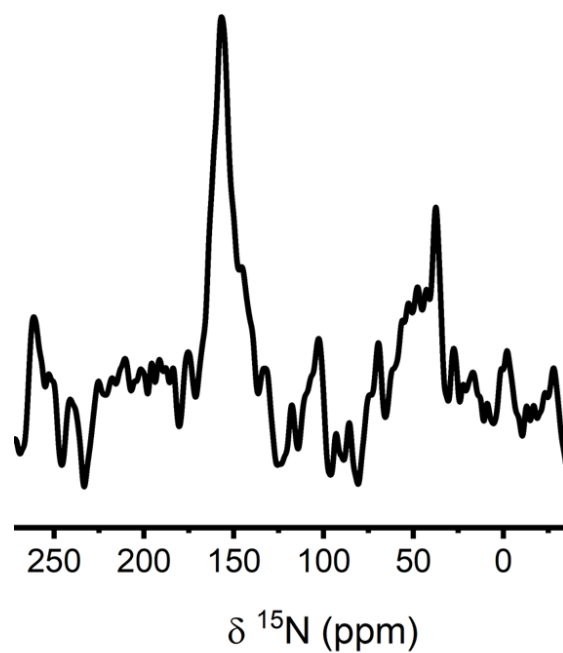


**Figure S19.**  $^1\text{H}$ - $^{15}\text{N}$  CP measurement of PDK403. Two nitrogen environments can be seen at 156 ppm and at 37 ppm. The environment at 37 ppm originates from T403 (see Figure S20) indicating residual monomer in the polymer. Spectrum was acquired at 11.7 T.

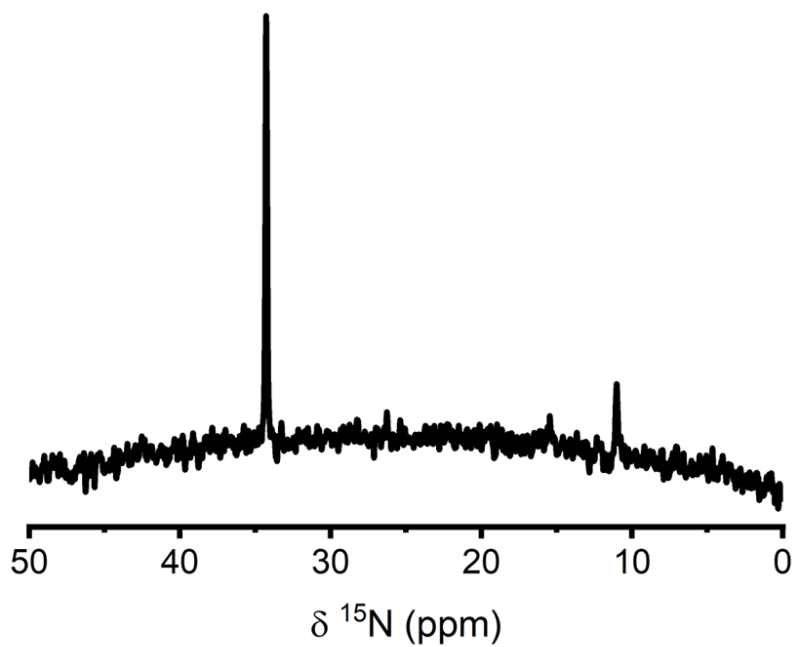


**Figure S20.**  $^{15}\text{N}$  zig spectrum of T403 in  $\text{DMSO-d}_6$ . The main peak resonates at 34 ppm with a small peak at 11 ppm. Spectrum was acquired at 14.1 T.

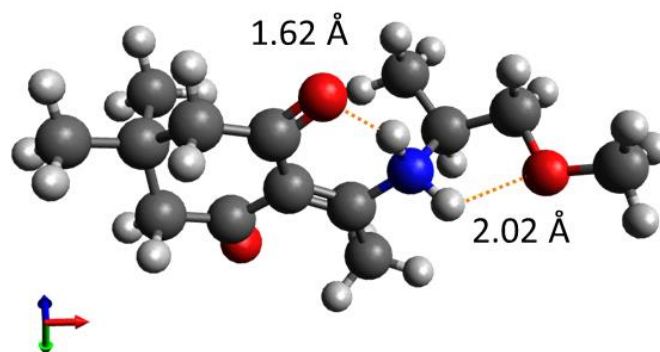


**Figure S21.** Molecular structure and hydrogen bond lengths for the proposed intermediate resonating at 8 ppm. Avogadro software was used for visualization.

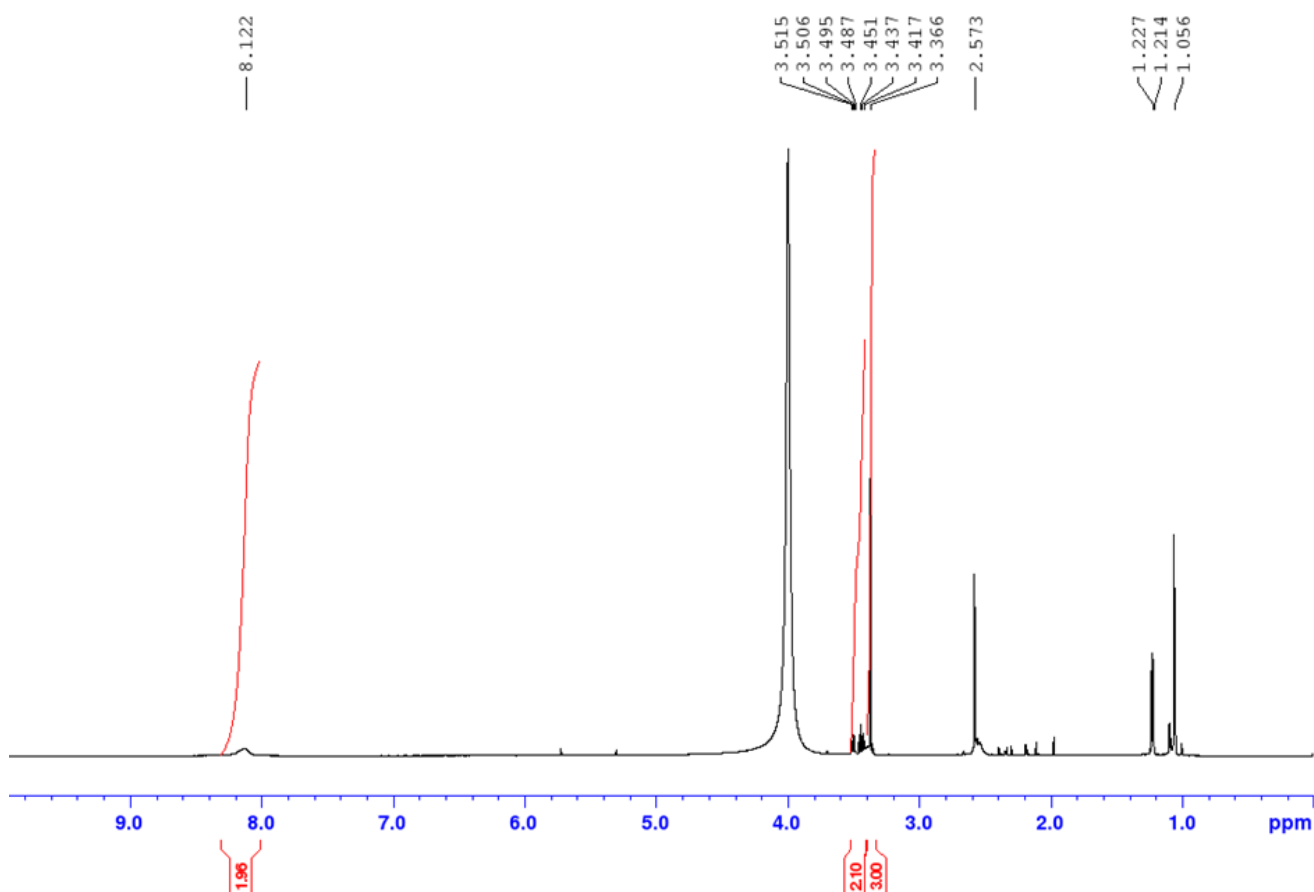


**Figure S22.** Relative integrations of  $^1\text{H}$  measurement of degraded DKE after 1 h in 5 M HCl, extracted with  $\text{DMSO-}d_6$ .  $\delta$   $^1\text{H}$ : 8 ppm 2H ( $\text{NH}_2^+$ ), 3.5 ppm 2H ( $\text{CH}_2\text{-O}$ ), and 3.42 ppm 3H ( $\text{O-CH}_3$ ). Spectrum was acquired at 11.7 T.

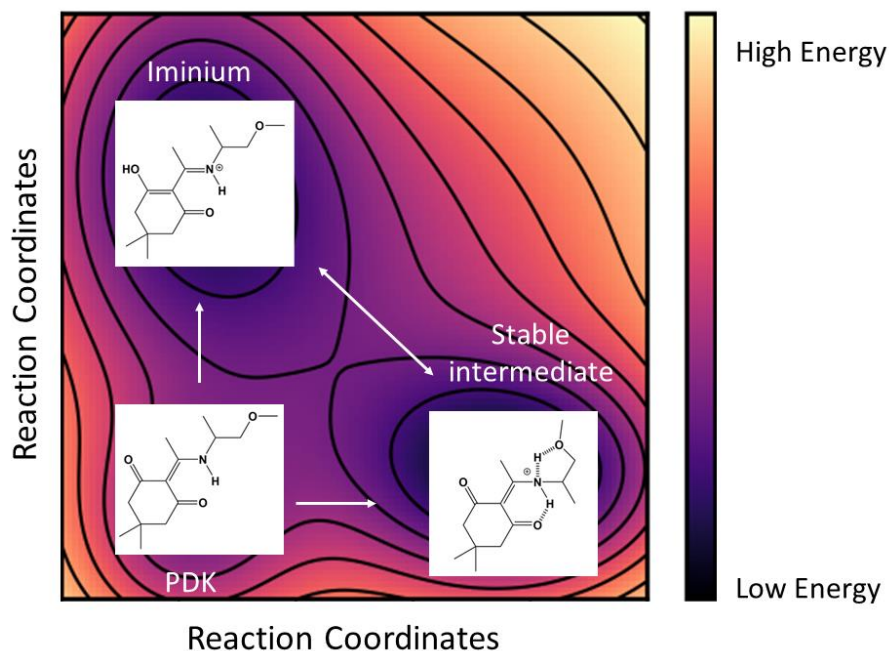


**Figure S23.** Schematic representation of an energy surface and the different pathways of deconstruction. Two local energy wells can be formed, one forming a protonated diketoenamine intermediate<sup>7,8</sup> and another forming a stable double ringed intermediate. Due to enhanced stability from the double ring structure, this intermediate is in a relative low energy well. As swelling proceeds, the chains stretch and strain, leading to distortion of the intermediate and disconnection of the hydrogen bond to return to the protonated N-H<sup>+</sup> intermediate hydrolysis pathway. After depolymerization has begun and chain deconstruction is ongoing, swelling and strain is reduced and the cyclic intermediate remains unreactive.

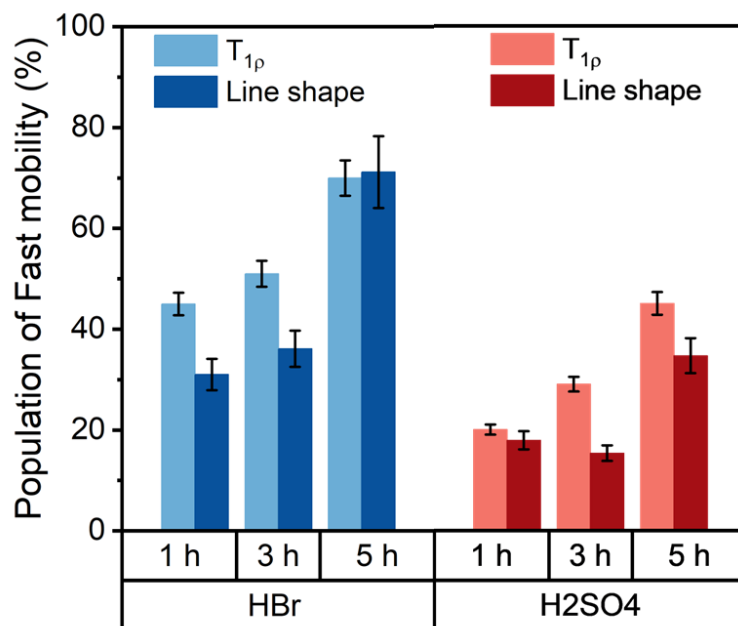


**Figure S24.** Integrated intensities of the fraction with fast mobility analyzed with line shape analysis (Figure 2c and 2d, dark blue and red) and with  $^1\text{H}$   $T_{1\rho}$  measurement (Figure 5a, light blue and red). Blue shades are data set of polymer deconstruction in 5 M HBr and red shades are for polymer deconstruction in 5 M  $\text{H}_2\text{SO}_4$ .

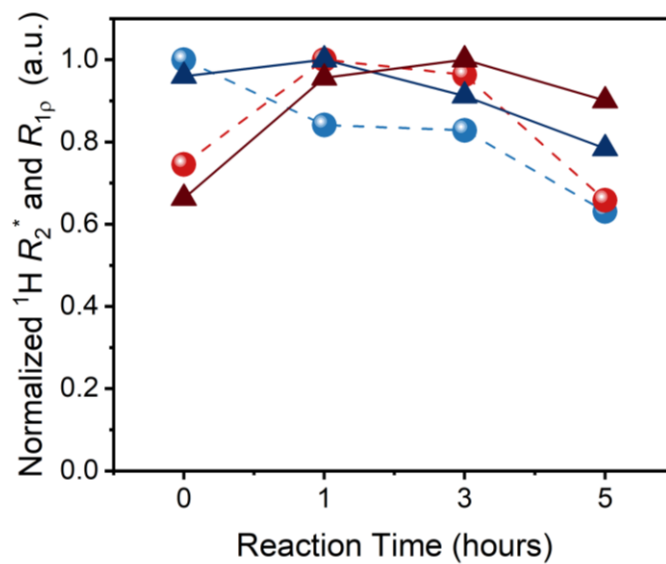


**Figure S25.** Proton linewidths converted to  $R_2^*$  ( $1/T_2^*$ ) as a function of reaction time, normalized for HBr (blue dot) and H<sub>2</sub>SO<sub>4</sub> (red dot). Fraction of larger  $R_{1\rho}$  ( $1/T_{1\rho}$ ) of residual polymer samples as a function of reaction time, normalized for HBr (blue triangles) and for H<sub>2</sub>SO<sub>4</sub> (red triangles).

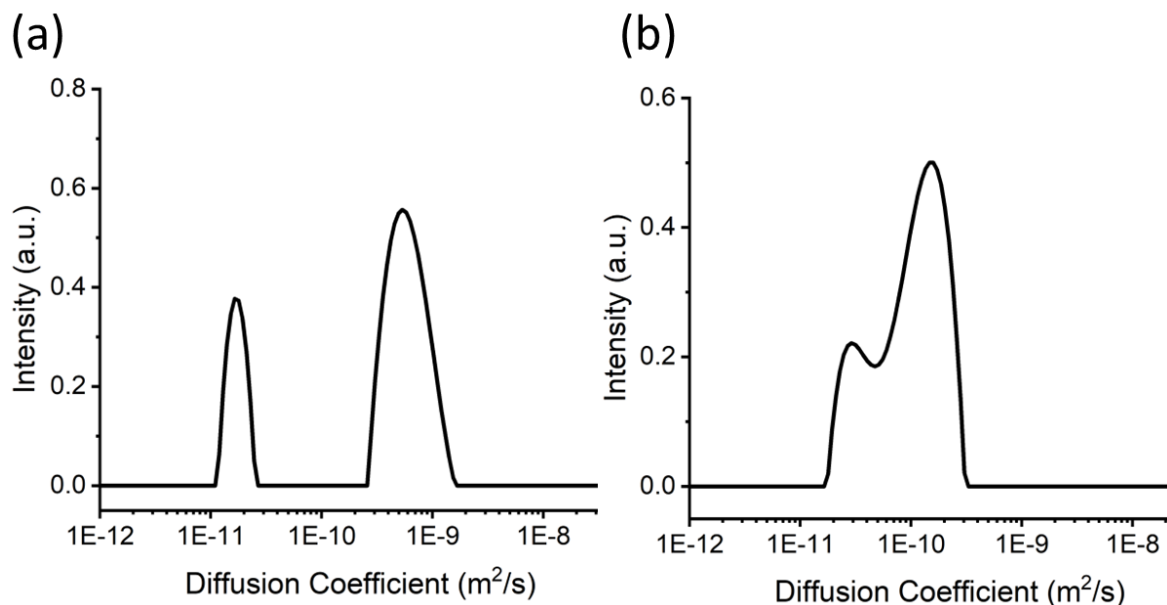


**Figure S26.** ILT analysis for <sup>1</sup>H PFG-NMR of swelled PDK403 (a) in D<sub>2</sub>O after a month and (b) in CDCl<sub>3</sub> after 12 hours.

#### *Swelling in non-acidic environments*

The ILT analysis of PDK403 in a non-acidic environment, in which no chemical reactions occur, isolates the effect of swelling on polymer motion. Visible swelling was observed when unreacted PDK403 was left in D<sub>2</sub>O for a month, resulting in increased resolution in <sup>1</sup>H NMR spectroscopy (Figure S2). <sup>1</sup>H PFG-NMR was performed and ILT analysis of the distribution of diffusion coefficient for the corresponding month-old sample was performed (Figure S26a). In addition, <sup>1</sup>H PFG-NMR and ILT analysis was carried out for PDK403 in CDCl<sub>3</sub> after 12 h of immersion (Figure S26b).

The ILT distribution of PDK403 in both D<sub>2</sub>O and CDCl<sub>3</sub> exhibits two distinct motions. The slow molecular motion in water, with the average diffusion coefficient of 2 × 10<sup>-11</sup> m<sup>2</sup>/s corresponds to the motion of the bulk polymer and the moderate motion ranging between 1 × 10<sup>-10</sup> to 1 × 10<sup>-9</sup> m<sup>2</sup>/s corresponds to the fraction of polymer chains that have undergone swelling and are splayed outwards of the more ordered bulk polymer. These polymer splays are more greatly affected by the mobility of the surrounding solvent than the confined bulk polymer. The self-diffusivity of H<sub>2</sub>O<sup>9</sup> is higher than the self-diffusivity of CHCl<sub>3</sub>,<sup>10</sup> affecting the faster moderate motion in D<sub>2</sub>O. Furthermore, since the D<sub>2</sub>O sample was immersed in the solvent for a significantly longer time, it

is evident that the polymer has faster molecular motion especially on the outer rim. Overall, polymer motion observed around  $10^{-11}$  to  $10^{-9}$  m<sup>2</sup>/s can be attributed to swelled polymer motion. This diffusivity is also observed in PDK403 in acidic conditions, specifically for polymer chain environments. The similarity between the overall polymer motion in non-acidic solvents (Figure S26) and polymer chain motion in acidic solvents (Figure 5c and 5d) indicates that the motion of the polymer backbone of PDK403 is the product of swelling.

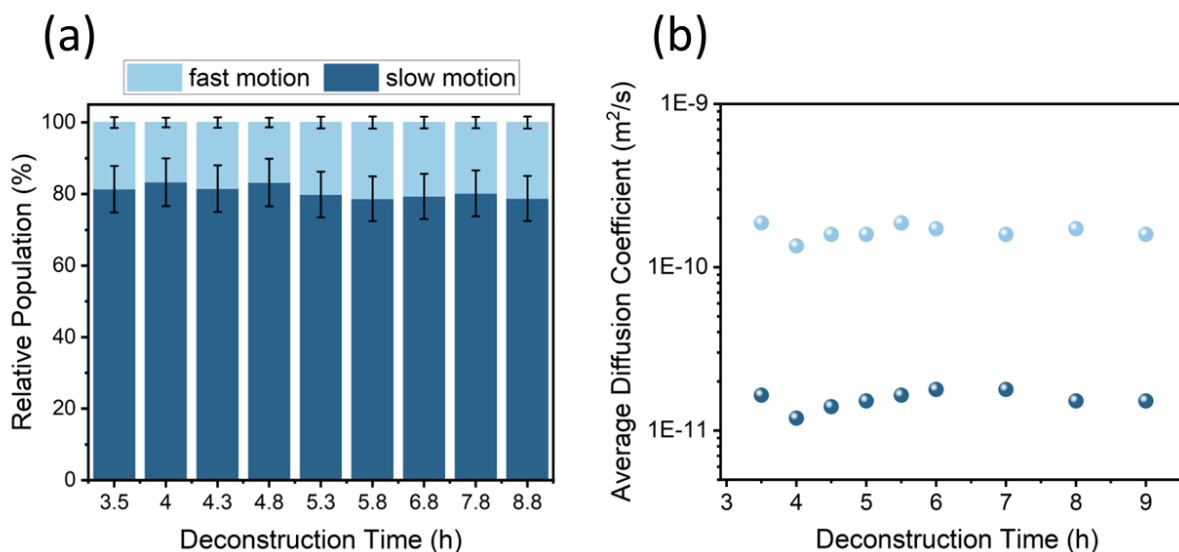


**Figure S27.** Quantification of polymer backbone motion in PDK403 in 5 M HBr based on ILT analysis presented in Figure 5c. (a) The relative population of protons with fast or slow motion as a function of deconstruction time. Relative population is calculated based on the integral under each curve in Figure 5c. (b) The average diffusion coefficient of fast and slow motion as a function of deconstruction time. The average diffusion coefficient was calculated as the corresponding diffusion coefficient to the maximum intensity of each peak in Figure 5c.

### *Polymer Chain Motion in DBr Acid*

We conclude from the previous section that the motion of polymer backbone in PDK403 is due to swelling. We focus on the relative population of the protons in the polymer backbone region that is exhibiting either slow or fast motion (Figure S27). Throughout the entire deconstruction process, the relative proton populations do not change significantly, always maintaining a ratio of 80% slow and 20% fast motion. This is significantly different from what is

observed in non-acidic solvents, such as in the case of  $\text{CDCl}_3$  where the distribution was closer to 30–70 % slow and fast (Figure S26). The lack of fast diffusing splayed polymer chains can be explained by a decrease in  $T_2$  relaxation seen in monomer chains, making them invisible to  $^1\text{H}$  spectroscopy. Therefore, although more extensive swelling happens during acidic reactions, sensitivity limits ILT analysis in acknowledging the transition of swelled polymer chains into monomer chains.

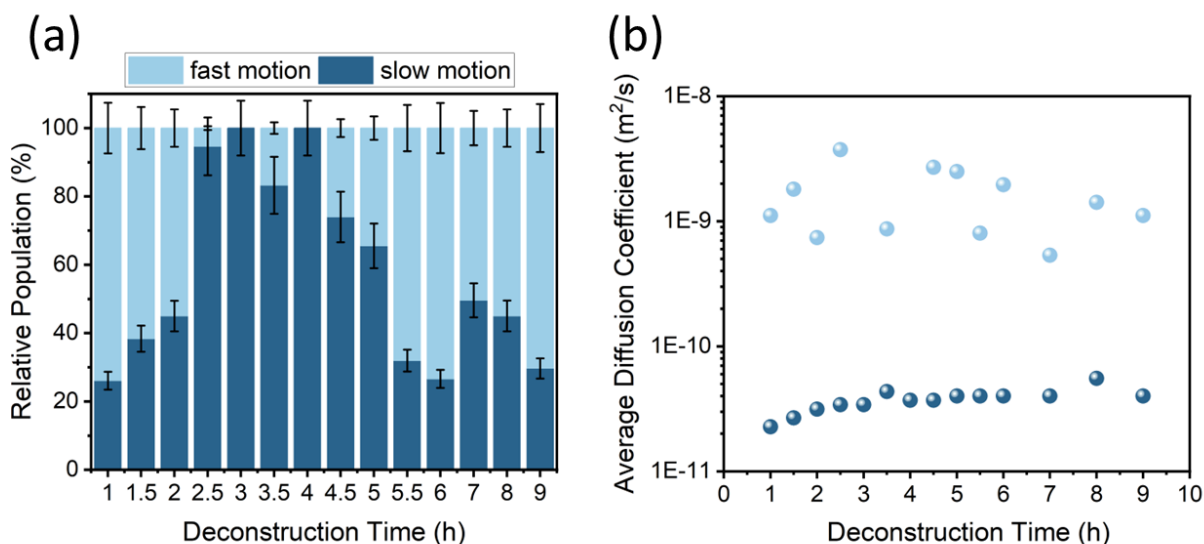


**Figure S28.** Quantification of reaction site motion of PDK403 in 5M HBr based on the ILT analysis presented in Figure 5d. (a) The relative population of protons that belong to fast or slow motion as a function of deconstruction time. Relative population is calculated based on the integral under each curve in Figure 5d. (b) The average diffusion coefficient of fast and slow motion as a function of deconstruction time. The average diffusion coefficient was calculated as the corresponding diffusion coefficient to the maximum intensity of each peak in Figure 5d.

#### *Reaction Site Motion in DBr Reaction*

Understanding the motion of the polymer deconstruction reaction site requires comprehending the heterogenous nature of the reaction as well as the complicated dynamics between the protons, water, and the reaction site. Quantification of the change in relative population of fast and slow motion (Figure S28) shows non-linearity in molecular diffusivity. Specifically, throughout deconstruction time of 1 – 9 h, we observe initially a dominating fast

motion, followed by an overall slow motion around 3.5 h, then a return to fast motion. We hypothesize that this non-linearity shows a transition in reaction site. Initially, most of the acid penetrates the outer layer, protonating the accessible amine sites and further expanding the polymer chains. However, during the slow-motion phase, the acid penetrates deeper into the polymer that is not yet swelled enough to reflect the faster motions. Eventually, with enough reaction and acid penetration, even the deeper regions of PDK403 are capable of exhibiting faster motion. We note that the definition of fast and slow motion varies between the reaction site and the polymer backbone. The reaction site slow motion has a diffusion coefficient of  $3 \times 10^{-11} \text{ m}^2/\text{s}$  which is of similar magnitude as the bulk polymer (an average of the bulk polymer's two motions). This reflects the effect of polymer backbone movement on the reaction site as well. However, the fast motion, with a diffusion coefficient of  $1 \times 10^{-9} \text{ m}^2/\text{s}$ , exhibits much faster movement, similar to small molecule mobility in acid.<sup>11</sup> More random distribution of the average diffusion coefficient is also observed in Figure S28b, likely due to multiple motions and or conformations such as attack of proton and water and the twisting of structure to allow those attacks.

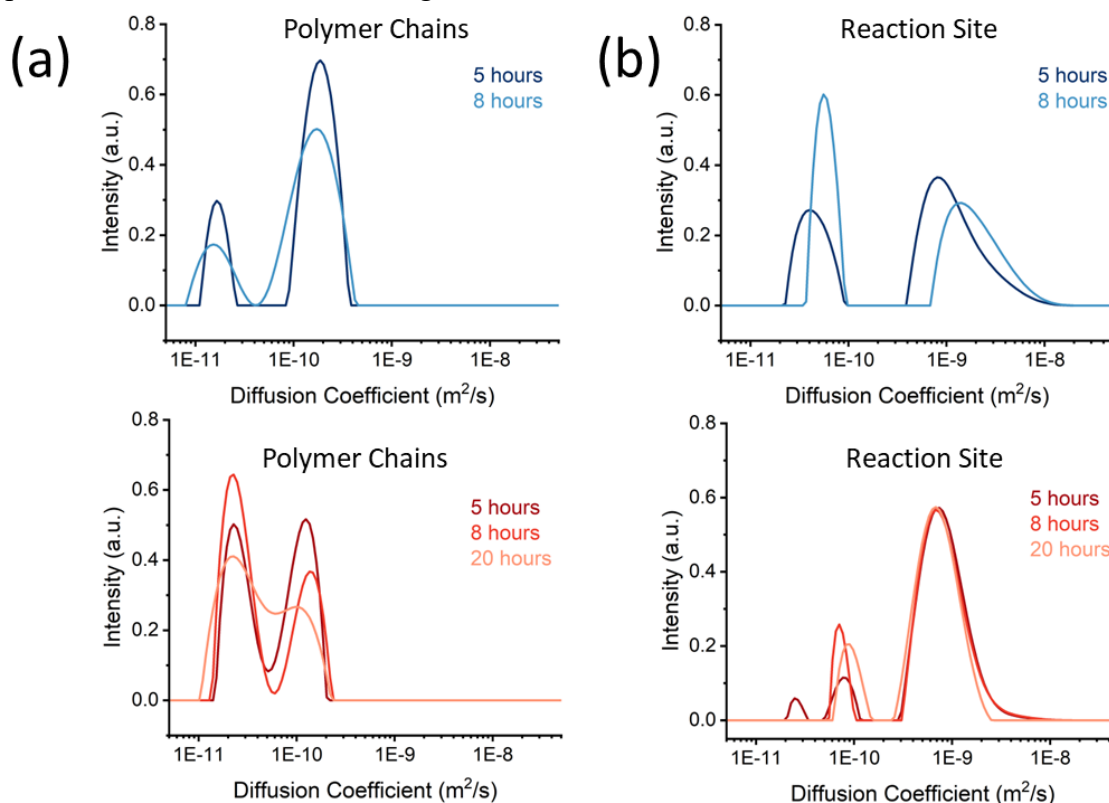


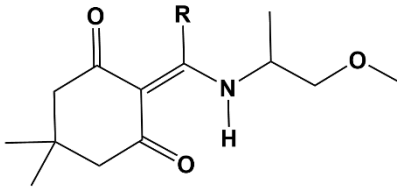
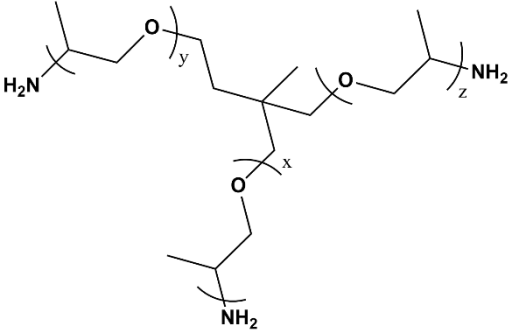
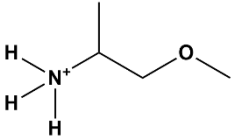
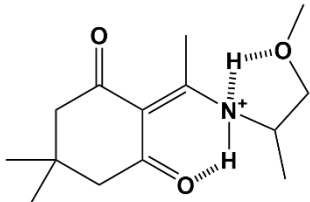
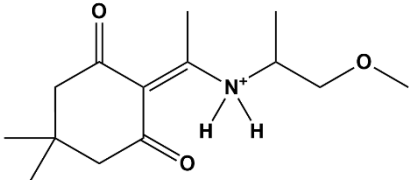
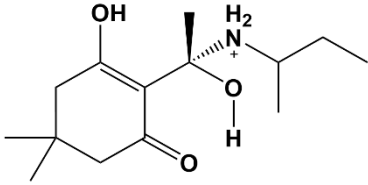
**Figure S29.** ILT analysis of diffusion of PDK403 in 5 M DBr/D<sub>2</sub>O (blue) and 5M D<sub>2</sub>SO<sub>4</sub>/D<sub>2</sub>O (red) (a) for polymer chain proton environment and (b) for the reaction site proton environment.

### *Polymer Diffusivity in DBr and D<sub>2</sub>SO<sub>4</sub> Deconstruction*

Additional comparable <sup>1</sup>H PFG-NMR measurements were performed to follow the diffusivity of degraded PDK403 in 5 M D<sub>2</sub>SO<sub>4</sub>. The resulting distribution of diffusion coefficient is shown for both acidic mediums (Figure S29). A significant proton signal that could be attenuated was acquired only after 5 h of deconstruction in D<sub>2</sub>SO<sub>4</sub>. This strongly displays the slow kinetics of polymer deconstruction in sulfuric acid.

The motion of polymer backbone chains in both acidic solutions is similar (see Table 6 for nominal diffusion coefficients). With increasing deconstruction time, we observe an increase in the distribution of diffusion coefficients and less separation between the two peaks which is expected since more regions of the polymers are undergoing swelling at different levels. Similarly, for the reaction site we see that PDK403 in D<sub>2</sub>SO<sub>4</sub> also undergoes reaction, as reflected by the presence of fast motion. The small fraction of slow-moving reaction site protons in D<sub>2</sub>SO<sub>4</sub> is explained by the lack of an effect of bulk polymer motion on this group. This further supports the formation of protonated amine in H<sub>2</sub>SO<sub>4</sub>, -NH<sup>+</sup>-, and the formation of an intermediate in HBr, bringing the reaction protons closer to the CH<sub>2</sub> chains.

**Table S1.** Proposed structures and DFT calculations of their  $^1\text{H}$  and  $^{15}\text{N}$  chemical shifts.

Name	Chemical structure	$\delta$ $^1\text{H}$ N-H bond (ppm)	$\delta$ $^{15}\text{N}$ (ppm)	Experiment/DFT
<b>DKE and PDK</b>		13.6	156	NMR (Figure S19)
		14.2	163	DFT
<b>T403</b>		3.3	34	NMR (Figure S20)
<b>N1</b>		7.5	59	DFT
<b>I1</b>		6.8 (H-O-C) 13.0 (H-O=C)	91.6	DFT
<b>I2</b>		H <sub>1</sub> 15.9 H <sub>2</sub> 4.1	89	DFT
<b>I3</b>		H <sub>1</sub> 5.5 H <sub>2</sub> 3.9	120	DFT

<b>I4</b>		$H_1$ 11.2 $H_2$ 3.6	99	DFT
<b>I5</b>		9.3	212	DFT
<b>I6</b>		14.2	218	DFT

**Table S2.** Summary of  $^1\text{H}$ - $^{15}\text{N}$  HSQC cross peaks of degraded PDK403 (Figure S18).

<b>Cross peak</b> ( $\delta$ $^1\text{H}$ / $^{15}\text{N}$ ppm)	<b>Proposed structure</b> (Table S1)	<b>Comments</b>
7.8 / 32	N1	This protonated amine has most likely undergone elimination but is still connected to the polymer. <sup>12</sup> (Figure S4)
8 / 45	I1	See main text
7.7 / 129	I3 and or I4	The first step of polymer deconstruction is the ionization of the nitrogen atom. This leads to the attack of water and the formation of an enol. An average proton chemical shift is expected due to fast exchange of the keto-enol bonds.
13.35 / 139	I2	The carbon double bond greatly affects the N-H chemical shift.
13.4 / 156	PDK	Although the measured sample was taken from the outer layers of the degraded polymer, there are still residual polymer N-H bonds. (Figure S19)
13.2 / 218	I5 and or I6	A charged nitrogen, double bonded to carbon gives a distinct chemical shift. The fast exchange of keto-enol states gives way to average proton chemical shift.

**Table S3.** Percentage of normalized integrated intensities of  $^1\text{H}$  Hahn echo spectra for degraded polymer in 5 M HBr acid (blue) and 5 M  $\text{H}_2\text{SO}_4$  acid (red).

<b>Deconstruction Time</b>	<b>Polymer (%)</b>		<b>NH<sup>+</sup> (%)</b>		<b>Intermediate (%)</b>		<b>Monomer (%)</b>	
<b>After 1 h</b>	69	> 95	4	4	10	-	17	< 1
<b>After 3 h</b>	64	91	9	5	11	-	16	4
<b>After 5 h</b>	28	87	11	5	12	-	49	8

Original spectra are presented in Figure 2c and 2d. Peaks were separated into four groups according to chemical shift and linewidth: polymer,  $\text{NH}^+$ , intermediate, and monomer.

**Table S4.**  $^1\text{H}$   $T_{1\rho}$  data for PDK403 and degraded polymer samples in 5 M HBr (blue) and 5 M  $\text{H}_2\text{SO}_4$  (red).

<b>Deconstruction Time</b>	<b>Short <math>T_{1\rho}</math> (<math>\mu\text{s}</math>)</b>		<b>Long <math>T_{1\rho}</math> (ms)</b>	
<b>PDK403</b>	530 (26%)		2.5 (74%)	
<b>After 1 h</b>	630 (45%)	395 (20%)	2.6 (55%)	3.8 (80%)
<b>After 3 h</b>	640 (51%)	410 (29%)	2.6 (49%)	2.3 (71%)
<b>After 5 h</b>	840 (70%)	600 (45%)	9.9 (30%)	2.4 (55%)

**Table S5.**  $^1\text{H}$   $T_2$  data for PDK403 and degraded polymer samples in 5 M HBr (blue) and 5 M  $\text{H}_2\text{SO}_4$  (red).

<b>Deconstruction Time</b>	<b>Short <math>T_2</math> (<math>\mu\text{s}</math>)</b>		<b>Long <math>T_2</math> (ms)</b>	
<b>PDK403</b>	280 (77%)		1.6 (23%)	
<b>After 1 h</b>	255 (66%)	270 (72%)	0.83 (34%)	0.89 (28%)
<b>After 3 h</b>	263 (63%)	285 (69%)	0.89 (37%)	0.90 (31%)
<b>After 5 h</b>	280 (59%)	310 (66%)	1.4 (41%)	0.93 (34%)

**Table S6.** Summary of average diffusion coefficients (D) for polymer chain diffusion in various systems.

<b>Chemical Environment</b>	<b>Reaction Medium</b>	<b>Slow motion (<math>10^{-10} \text{ m}^2 \text{ s}^{-1}</math>)</b>	<b>Moderate motion (<math>10^{-10} \text{ m}^2 \text{ s}^{-1}</math>)</b>	<b>Fast motion (<math>10^{-10} \text{ m}^2 \text{ s}^{-1}</math>)</b>
Reaction Site	DBr/D <sub>2</sub> O <sup>(1)</sup>		0.37	12.0
Polymer Chains		0.16	1.7	
Reaction Site	D <sub>2</sub> SO <sub>4</sub> /D <sub>2</sub> O <sup>(1)</sup>		0.78	7.4
Polymer Chains		0.23	1.2	
Polymer Chains	D <sub>2</sub> O <sup>(2)</sup>	0.18		5.4
Polymer Chains	CDCl <sub>3</sub> <sup>(3)</sup>	0.29	1.6	

(1) Diffusion coefficient distribution was averaged over a course of 8 h of deconstruction time.

(2) PDK403 was immersed in D<sub>2</sub>O for a month prior to PFG measurement.

(3) PDK403 was immersed in CDCl<sub>3</sub> for 12 hours prior to PFG measurement.

Table S6 summarizes the results of the diffusivity studies according to varying levels of motion. We particularly emphasize that the motion of the polymer chains of PDK403 in acidic conditions resemble the motion of polymers in non-acidic solvents, shedding light on the mobility of swelled polymers. We attribute the slow motion of polymer chains to the bulk movement and the fast motion to the splayed branches, under the influence of solvent motion. We also acknowledge that the behavior of the reaction site is significantly different from the polymer branch, mainly exhibiting non-linear, random motion as a result of intercalation of varying factors of deconstruction.

## References

- (1) Karplus, M. Contact Electron-Spin Coupling of Nuclear Magnetic Moments. *J Chem Phys* **1959**, *30* (1), 11–15. <https://doi.org/10.1063/1.1729860>.
- (2) Edison, A. S.; Schroeder, F. C. 9.06 NMR-Small Molecules and Analysis of Complex Mixtures. In *Comprehensive Natural Products*; Hung-Wen (Ben) Liu, L. M., Ed.; Elsevier, 2010; Vol. II, pp 169–196.
- (3) Liu, Q.; Zhu, M. Determination of Molar Ratio of Primary Secondary and Tertiary Amines in Polymers by Applying Derivatization and NMR Spectroscopy. *Polym Test* **2016**, *56*, 174–179. <https://doi.org/10.1016/j.polymertesting.2016.10.013>.
- (4) Forse, A. C.; Milner, P. J.; Lee, J. H.; Redfearn, H. N.; Oktawiec, J.; Siegelman, R. L.; Martell, J. D.; Dinakar, B.; Porter-Zasada, L. B.; Gonzalez, M. I.; Neaton, J. B.; Long, J. R.; Reimer, J. A. Elucidating CO<sub>2</sub> Chemisorption in Diamine-Appended Metal-Organic Frameworks. *J Am Chem Soc* **2018**, *140* (51), 18016–18031. <https://doi.org/10.1021/jacs.8b10203>.
- (5) Hansen, P. E. A Spectroscopic Overview of Intramolecular Hydrogen Bonds of NH ... O,S,N Type. *Molecules* **2021**, *26* (9), 2409. <https://doi.org/10.3390/molecules26092409>.
- (6) Froimowicz, P.; Zhang, K.; Ishida, H. Intramolecular Hydrogen Bonding in Benzoxazines: When Structural Design Becomes Functional. *Chemistry - A European Journal* **2016**, *22* (8), 2691–2707. <https://doi.org/10.1002/chem.201503477>.
- (7) Dailing, E. A.; Khanal, P.; Epstein, A. R.; Demarteau, J.; Persson, K. A.; Helms, B. A. Circular Polydiketoenamine Elastomers with Exceptional Creep Resistance via Multivalent Cross-Linker Design. *ACS Cent Sci* **2024**, *10* (1), 54–64. <https://doi.org/10.1021/acscentsci.3c01096>.
- (8) Demarteau, J.; Epstein, A. R.; Christensen, P. R.; Abubekero, M.; Wang, H.; Teat, S. J.; Seguin, T. J.; Chan, C. W.; Scown, C. D.; Russell, T. P.; Keasling, J. D.; Persson, K. A.; Helms, B. A. Circularity in Mixed-Plastic Chemical Recycling Enabled by Variable Rates of Polydiketoenamine Hydrolysis. *Sci. Adv* **2022**, *8*, 8823.
- (9) Mills, R. Self-Diffusion in Normal and Heavy Water in the Range 1–45°. *J Phys Chem* **1973**, *77* (5), 685–688.
- (10) Meckl, S.; Zeidler, M. D. Self-Diffusion Measurements of Ethanol and Propanol. *Mol Phys* **1988**, *63* (1), 85–95. <https://doi.org/10.1080/00268978800100081>.
- (11) Hua, M.; Peng, Z.; Guha, R.; Ruan, X.; Ng, K. C.; Demarteau, J.; Haber, S.; Fricke, S. N.; Reimer, J. A.; Salmeron, M.; Persson, K. A.; Wang, C.; Helms, B. A. Mechanochemically Accelerated Deconstruction of Chemically Recyclable Plastics. *ChemRxiv* **2023**. <https://doi.org/10.26434/chemrxiv-2023-rf93d>.

- (12) Lambert, J. B.; Binsch, G.; Roberts, J. D. Nitrogen-15 Magnetic Resonance Spectroscopy. I. Chemical Shifts. *Proc Natl Acad Sci U S A* **1964**, *51*, 735–737. <https://doi.org/10.1073/pnas.51.5.735>.

- (5) Beedle, A. E. M.; Mora, M.; Davis, C. T.; Snijders, A. P.; Stirnemann, G.; Garcia-Manyes, S. Forcing the Reversibility of a Mechanochemical Reaction. *Nat. Commun.* **2018**, *9* (1), 3155.
- (6) Christensen, P. R.; Scheuermann, A. M.; Loeffler, K. E.; Helms, B. A. Closed-Loop Recycling of Plastics Enabled by Dynamic Covalent Diketoenamine Bonds. *Nat. Chem.* **2019**, *11* (5), 442–448.
- (7) Demarteau, J.; Cousineau, B.; Wang, Z.; Bose, B.; Cheong, S.; Lan, G.; Baral, N. R.; Teat, S. J.; Scown, C. D.; Keasling, J. D.; Helms, B. A. Biorenewable and Circular Polydiketoenamine Plastics. *Nat. Sustainable* **2023**, *6* (11), 1426–1435.
- (8) Chu, M.; Liu, Y.; Lou, X.; Zhang, Q.; Chen, J. Rational Design of Chemical Catalysis for Plastic Recycling. *ACS Catal.* **2022**, *12*, 4659–4679.
- (9) Young, J. B.; Hughes, R. W.; Tamura, A. M.; Bailey, L. S.; Stewart, K. A.; Sumerlin, B. S. Bulk Depolymerization of Poly(Methyl Methacrylate) via Chain-End Initiation for Catalyst-Free Reversion to Monomer. *Chem* **2023**, *9* (9), 2669–2682.
- (10) Ellis, L. D.; Rorrer, N. A.; Sullivan, K. P.; Otto, M.; McGeehan, J. E.; Román-Leshkov, Y.; Wierckx, N.; Beckham, G. T. Chemical and Biological Catalysis for Plastics Recycling and Upcycling. *Nat. Res.* **2021**, *4*, 539–556.
- (11) Metzke, F. K.; Sant, S.; Meng, Z.; Klok, H. A.; Kaur, K. Swelling-Activated, Soft Mechanochemistry in Polymer Materials. *Langmuir* **2023**, *39*, 3546–3557.
- (12) Lee, C. K.; Diesendruck, C. E.; Lu, E.; Pickett, A. N.; May, P. A.; Moore, J. S.; Braun, P. V. Solvent Swelling Activation of a Mechanophore in a Polymer Network. *Macromolecules* **2014**, *47* (8), 2690–2694.
- (13) Demarteau, J.; Epstein, A. R.; Christensen, P. R.; Abubekkerov, M.; Wang, H.; Teat, S. J.; Seguin, T. J.; Chan, C. W.; Scown, C. D.; Russell, T. P.; Keasling, J. D.; Persson, K. A.; Helms, B. A. Circularity in Mixed-Plastic Chemical Recycling Enabled by Variable Rates of Polydiketoenamine Hydrolysis. *Sci. Adv.* **2022**, *8*, 8823.
- (14) Epstein, A. R.; Demarteau, J.; Helms, B. A.; Persson, K. A. Variable Amine Spacing Determines Depolymerization Rate in Polydiketoenamines. *J. Am. Chem. Soc.* **2023**, *145* (14), 8082–8089.
- (15) Hua, M.; Peng, Z.; Guha, R. D.; Ruan, X.; Ng, K. C.; Demarteau, J.; Haber, S.; Fricke, S. N.; Reimer, J. A.; Salmeron, M. B.; Persson, K. A.; Wang, C.; Helms, B. A. Mechanochemically Accelerated Deconstruction of Chemically Recyclable Plastics. *Sci. Adv.* **2024**, *10*, 3801.
- (16) Fricke, S. N.; Haber, S.; Hua, M.; Salgado, M.; Helms, B. A.; Reimer, J. A. Magnetic Resonance Insights into the Heterogeneous, Fractal-like Kinetics of Chemically Recyclable Polymers. *Sci. Adv.* **2024**, *10*, 568.
- (17) Bruce, E. E.; Van Der Vegt, N. F. A. Molecular Scale Solvation in Complex Solutions. *J. Am. Chem. Soc.* **2019**, *141* (33), 12948–12956.
- (18) Johnson, R. L.; Schmidt-Rohr, K. Quantitative Solid-State <sup>13</sup>C NMR with Signal Enhancement by Multiple Cross Polarization. *J. Magn. Reson.* **2014**, *239*, 44–49.
- (19) Sinnaeve, D. The Stejskal-Tanner Equation Generalized for Any Gradient Shape-An Overview of Most Pulse Sequences Measuring Free Diffusion. *Concepts Magn. Reson., Part A: Bridging Educ. Res.* **2012**, *40A* (2), 39–65.
- (20) Hansen, P. C.; Jensen, T. K.; Rodriguez, G. An Adaptive Pruning Algorithm for the Discrete L-Curve Criterion. *J. Comput. Appl. Math.* **2007**, *198* (2), 483–492.
- (21) Fung, B. M.; Khitritin, A. K.; Ermolaev, K. An Improved Broadband Decoupling Sequence for Liquid Crystals and Solids. *J. Magn. Reson.* **2000**, *142*, 97–101.
- (22) Liu, H.; Zhou, X.; Chen, Q.; Zhang, S. Accurate Quantitative and Maximum Cross Polarization via Multiple Ramped Contacts. *Chem. Phys. Lett.* **2017**, *679*, 233–236.
- (23) Brownbill, N. J.; Sprick, R. S.; Bonillo, B.; Pawsey, S.; Aussenac, F.; Fielding, A. J.; Cooper, A. I.; Blanc, F. Structural Elucidation of Amorphous Photocatalytic Polymers from Dynamic Nuclear Polarization Enhanced Solid State NMR. *Macromolecules* **2018**, *51* (8), 3088–3096.
- (24) Bertani, P.; Raya, J.; Bechinger, B. 15N Chemical Shift Referencing in Solid State NMR. *Solid State Nucl. Magn. Reson.* **2014**, *61–62*, 15–18.
- (25) Massiot, D.; Fayon, F.; Capron, M.; King, I.; Le Calvé, S.; Alonso, B.; Durand, J. O.; Bujoli, B.; Gan, Z.; Hoatson, G. Modelling One- and Two-Dimensional Solid-State NMR Spectra. *Magn. Reson. Chem.* **2002**, *40* (1), 70–76.
- (26) Frisch, M. J.; Trucks, G. W.; Schlegel, H. B.; Scuseria, G. E.; Robb, M. A.; Cheeseman, J. R.; Scalmani, G.; Barone, V.; Petersson, G. A.; Nakatsuji, H.; Li, X.; Caricato, M.; Marenich, A. V.; Bloino, J.; Janesko, B. G.; Gomperts, R.; Mennucci, B.; Hratchian, H. P.; Ortiz, J. V.; Izmaylov, A. F.; Sonnenberg, J. L.; Williams-Young, D.; Ding, F.; Lipparini, F.; Egidi, F.; Goings, J.; Peng, B.; Petrone, A.; Henderson, T.; Ranasinghe, D.; Zakrzewski, V. G.; Gao, J.; Rega, N.; Zheng, G.; Liang, W.; Hada, M.; Ehara, M.; Toyota, K.; Fukuda, R.; Hasegawa, J.; Ishida, M.; Nakajima, T.; Honda, Y.; Kitao, O.; Nakai, H.; Vreven, T.; Throssell, K.; Montgomery, J. A., Jr.; Peralta, J. E.; Ogliaro, F.; Bearpark, M. J.; Heyd, J. J.; Brothers, E. N.; Kudin, K. N.; Staroverov, V. N.; Keith, T. A.; Kobayashi, R.; Normand, J.; Raghavachari, K.; Rendell, A. P.; Burant, J. C.; Iyengar, S. S.; Tomasi, J.; Cossi, M.; Millam, J. M.; Klene, M.; Adamo, C.; Cammi, R.; Ochterski, J. W.; Martin, R. L.; Morokuma, K.; Farkas, O.; Foresman, J. B.; Fox, D. J. *Gaussian 16*, Revision C.01; Gaussian, Inc.: Wallingford CT, 2016.
- (27) Grimme, S.; Antony, J.; Ehrlich, S.; Krieg, H. A Consistent and Accurate Ab Initio Parametrization of Density Functional Dispersion Correction (DFT-D) for the 94 Elements H-Pu. *J. Chem. Phys.* **2010**, *132* (15), 154104–154119.
- (28) Becke, A. D. Density-Functional Thermochemistry. III. The Role of Exact Exchange. *J. Chem. Phys.* **1993**, *98* (7), 5648–5652.
- (29) Chai, J.; Head-Gordon, M.; Head-Gordon, M. Long-Range Corrected Hybrid Density Functionals with Damped Atom-Atom Dispersion Corrections. *Phys. Chem. Chem. Phys.* **2008**, *10* (44), 6615–6620.
- (30) Grimme, S. Supramolecular Binding Thermodynamics by Dispersion-Corrected Density Functional Theory. *Chem.—Eur. J.* **2012**, *18* (32), 9955–9964.
- (31) Batamack, P.; Fraissard, J. Proton NMR Studies on Concentrated Aqueous Sulfuric Acid Solutions and Nafion-H. *Catal. Lett.* **1997**, *49*, 129–136.
- (32) Lambert, J. B.; Binsch, G.; Roberts, J. D. Nitrogen-15 Magnetic Resonance Spectroscopy. I. Chemical Shifts. *Proc. Natl. Acad. Sci. U.S.A.* **1964**, *51*, 735–737.
- (33) Hansen, P. E. A Spectroscopic Overview of Intramolecular Hydrogen Bonds of NH...O,S,N Type. *Molecules* **2021**, *26* (9), 2409.
- (34) Froimowicz, P.; Zhang, K.; Ishida, H. Intramolecular Hydrogen Bonding in Benzoxazines: When Structural Design Becomes Functional. *Chem.—Eur. J.* **2016**, *22* (8), 2691–2707.
- (35) Horii, F. Chapter 3 NMR Relaxations and Dynamics. In *Solid State NMR of Polymers*; Ando, I., Asakura, T., Eds.; Elsevier Science B.V, 1998; Vol. 84.
- (36) Kowalewski, J.; Mäler, L. *Nuclear Spin Relaxation in Liquids: Theory, Experiments, and Applications*, 6th ed.; Taylor & Francis: New York, 2006.
- (37) Fukushima, E.; Roeder, S. B. W. *Experimental Pulse NMR: A Nuts and Bolts Approach*; Addison-Wesley Pub. Co., 1981.